Human Molecular Genetics, 2012, Vol. 21, No. 22 ***4857–4875***
doi:10.1093/hmg/dds322
Advance Access published on August 6, 2012

Mutant human APP exacerbates pathology in a mouse model of NPC and its reversal by a β-cyclodextrin

Mahua Maulik[1,3,4], Bibaswan Ghoshal[2], John Kim[3], Yanlin Wang[2,3], Jing Yang[3], David Westaway[1,3,4] and Satyabrata Kar[1,2,3,4,*]

[1]Department of Medicine (Neurology), [2]Department of Psychiatry, [3]Centre for Prions and Protein Folding Diseases, and [4]Centre for Neuroscience, University of Alberta, Edmonton, AB T6G 2M8, Canada

Received May 6, 2012; Revised July 21, 2012; Accepted July 31, 2012

Niemann-Pick type C (NPC) disease, an autosomal recessive disorder caused primarily by loss-of-function mutations in *NPC1* gene, is characterized neuropathologically by intracellular cholesterol accumulation, gliosis and neuronal loss in selected brain regions. Recent studies have shown that NPC disease exhibits intriguing parallels with Alzheimer's disease (AD), including the presence of tau-positive neurofibrillary tangles (NFTs) and β-amyloid (Aβ)-related peptides in vulnerable brain regions. Since enhanced cholesterol level, which acts as a risk factor for AD, can increase Aβ production by regulating amyloid precursor protein (APP) metabolism, it is possible that APP overexpression can influence cholesterol-regulated NPC pathology. We have addressed this issue in a novel bigenic mice (ANPC) generated by crossing heterozygous Npc1-deficient mice with mutant human APP transgenic mice. These mice exhibited decreased lifespan, early object memory and motor impairments, and exacerbated glial pathology compared with other littermates. Neurodegeneration observed in the cerebellum of ANPC mice was found to be accelerated along with a selective increase in the phosphorylation/cleavage of tau protein. Additionally, enhanced levels/activity of cytosolic cathepsin D together with cytochrome c and Bcl-2-associated X protein suggest a role for the lysosomal enzyme in the caspase-induced degeneration of neurons in ANPC mice. The reversal of cholesterol accretion by 2-hydroxypropyl-β-cyclodextrin (2-HPC) treatment increased longevity and attenuated behavioral/pathological abnormalities in ANPC mice. Collectively, our results reveal that overexpression of APP in Npc1-deficient mice can negatively influence longevity and a wide spectrum of behavioral/neuropathological abnormalities, thus raising the possibility that APP and NPC1 may interact functionally to regulate the development of AD and NPC pathologies.

INTRODUCTION

Niemann-Pick type C (NPC) disease is an autosomal recessive neurovisceral disorder characterized by abnormal accumulation of unesterified cholesterol and glycosphingolipids within the endosomal–lysosomal (EL) system in a number of tissues including the brain. These defects in cholesterol sequestration trigger widespread neurological deficits such as ataxia, seizures and dementia that eventually lead to premature death (1,2). In majority of the cases, NPC disease is caused by loss-of-function mutations in the *NPC1* gene, which encodes a transmembrane glycoprotein implicated in the intracellular transport of cholesterol (3,4). Neuropathologically, NPC is characterized by the accumulation of unesterified cholesterol, activation of glial cells and presence of intracellular tau-positive neurofibrillary tangles (NFTs). Loss of neurons is evident primarily in the prefrontal cortex, thalamus and cerebellum but not in the hippocampus (5,6). Some studies have also shown that levels of β-amyloid (Aβ)-related peptides are increased in the vulnerable brain regions (7) as well as in the cerebrospinal fluid (8), while extracellular deposition of the peptide was apparent in patients with ε4 genotype of

*To whom correspondence should be addressed at: Centre for Prions and Protein Folding Diseases, Departments of Medicine (Neurology) and Psychiatry, University of Alberta, Edmonton, AB T6G 2M8, Canada. Tel: +1 780 492 9357; Fax: +1 780 492 9352; E-mail: skar@ualberta.ca

apolipoprotein E (APOE), which serves as a protein carrier for cholesterol (9). Interestingly, Balb/cNctr-Npc$^{N/N}$ mice due to spontaneous mutations in the *Npc1* gene (Npc-null) are found to recapitulate most of the human pathology, except for the formation of NFTs (10,11).

A number of recent studies have shown that NPC disease exhibits some intriguing parallels with the Alzheimer's disease (AD), the most common type of senile dementia affecting the elderly people. Neuropathologically, AD is characterized by the presence of NFTs, Aβ-containing neuritic plaques, gliosis and the loss of neurons primarily in the hippocampus, cortex and certain subcellular nuclei such as basal forebrain cholinergic neurons (12–14). The pathological changes observed in AD brains are believed to be triggered by *in vivo* accumulation of Aβ peptides derived from amyloid precursor protein (APP). The AD pathology, unlike NPC disease, is not associated with widespread intracellular accumulation of free cholesterol or loss of neurons in the cerebellum. Additionally, development of AD which occurs mostly after 65 years of age does not lead to ataxia as observed in NPC disease (2,6,13,14). Notwithstanding the differences, the striking parallels that exist between AD with NPC include (i) the presence of structurally and immunologically similar tau-positive NFTs (15,16), (ii) influence of ε4 isoform of APOE in promoting disease pathology (9,17,18) and (iii) endosomal abnormalities associated with accumulation of cleaved APP and/or Aβ peptides in vulnerable neurons (19). Recently, alteration of NPC1 mRNA/protein has been reported in vulnerable regions of AD brains indicating a functional link between NPC1 dysfunction and AD (20). Although cholesterol is not sequestered in AD as observed in NPC pathology, there is evidence that high cholesterol level increases the risk of AD (21,22) and neurons bearing NFTs exhibit higher levels of free cholesterol in AD brains (23). Many lines of experimental evidence further suggest that alteration in cholesterol homeostasis can influence APP metabolism, whereas changes in the level/expression of APP can also lead to altered cholesterol metabolism (24–27). These results *albeit* promote convergence of factors regulating NPC and AD pathologies, very little is currently known about the interaction between the NPC1 and APP.

Transgenic mice overexpressing mutant APP are known to recapitulate amyloid deposits and spatial learning deficits but do not exhibit overt loss of neurons as seen in AD brains (28–31). Earlier studies have shown that the up-regulating cholesterol level can exacerbate behavior and cellular pathology, whereas the decreasing cholesterol level can have opposite effects in these mice (24,27). However, it remains unclear how APP overexpression can influence behavior and pathological features, particularly the tau pathology and neurodegeneration that lie downstream of altered APP and cholesterol metabolisms, in Npc-null mice. We addressed this issue by using a new line of bigenic ANPC mice generated by crossing mutant human APP transgenic mice (29) with heterozygous Npc1-deficient mice (32). Our results clearly show that overexpression of APP in the presence of intracellular cholesterol accumulation can decrease longevity, accelerate the onset of behavioral abnormalities and exacerbate glial pathology as well as degeneration of neurons that show preferential vulnerability to cholesterol accumulation in NPC disease. To establish the significance of cholesterol, we treated ANPC mice with the sterol binding agent 2-hydroxypropyl-β-cyclodextrin (2-HPC) that has been shown to promote movement of the sequestered cholesterol from lysosomes to the metabolically active pool in various experimental paradigms (33–35). Our results clearly reveal that dispersal of cholesterol by 2-HPC treatment can not only prolong the lifespan but also can significantly reverse the behavioral and pathological abnormalities in ANPC mice, thus providing a strong functional link between APP and NPC1 genes that may interact in regulating both AD and NPC pathologies.

RESULTS

Generation of bigenic ANPC mice

To determine how overexpression of APP can influence pathological changes triggered by intracellular accumulation of cholesterol, we generated a novel bigenic ANPC mouse line (APP-Tg and Npc-null: APP$^{+/0}$Npc1$^{-/-}$) by crossing mutant human APP transgenic (APP-Tg: APP$^{+/0}$Npc1$^{+/+}$) with heterozygous Npc1-deficient (APP$^{0/0}$Npc1$^{+/-}$) mice (Fig. 1A). Our immunoblotting analysis revealed that APP holoprotein levels in ANPC mice were similar to APP-Tg and double heterozygous (Dhet: APP$^{+/0}$Npc1$^{+/-}$) mice but were markedly higher compared with wild-type (WT: APP$^{0/0}$Npc1$^{+/+}$) and homozygous Npc-null mice (Npc-null: APP$^{0/0}$Npc1$^{-/-}$), as expected (Fig. 1B). Npc1 protein levels did not differ between WT and APP-Tg mice, and as anticipated, the Dhet mice showed ∼50% reduction, while Npc-null and ANPC mice did not exhibit detectable levels of this protein (Fig. 1B). ANPC mice had a maximum of 77-day lifespan, with the mortality rate increasing drastically from the 55 days onward (Fig. 1C). Npc-null mice, as reported earlier (36), exhibited a reduced lifespan with only ∼30% of the animals alive past the 90-day censor date in our colony. The majority (>90%) of APP-Tg and Dhet mice, on the other hand, survived past the censor date, whereas the WT mice had no recorded deaths within the study period. Thus, the bigenic ANPC mice had a significantly reduced lifespan compared with WT, APP-Tg, Dhet or Npc-null mutants (Fig. 1C). Additionally, the ANPC mice reached a maximum body weight of ∼12 g by 6 weeks, which was ∼30% less compared with other lines of mice, and then declined progressively until death (Fig. 1D).

Accelerated object recognition memory and motor deficits

To determine whether overexpression of APP in Npc-null mice can influence cognitive performance, we evaluated all five genotypes at 4, 7 and 10 weeks of age in an object recognition memory test (Fig. 2A). The performance of WT, APP-Tg, Dhet, Npc-null and ANPC mice did not differ significantly at 4 weeks of age (data not shown). The ANPC mice, however, exhibited significant deficits in the object memory index (MI) at 7 and 10 weeks, whereas APP-Tg, Dhet and Npc-null mice showed a reduced MI only at 10 weeks (Fig. 2A). Loss of Npc1 function is known to impair motor ability in Npc-null mice (37). To examine this effect, we first tested mice of all five genotypes at 4, 7 and 10 weeks of age for their spontaneous locomotor activity (walking, rearing and periods of inactivity) in open-field tests

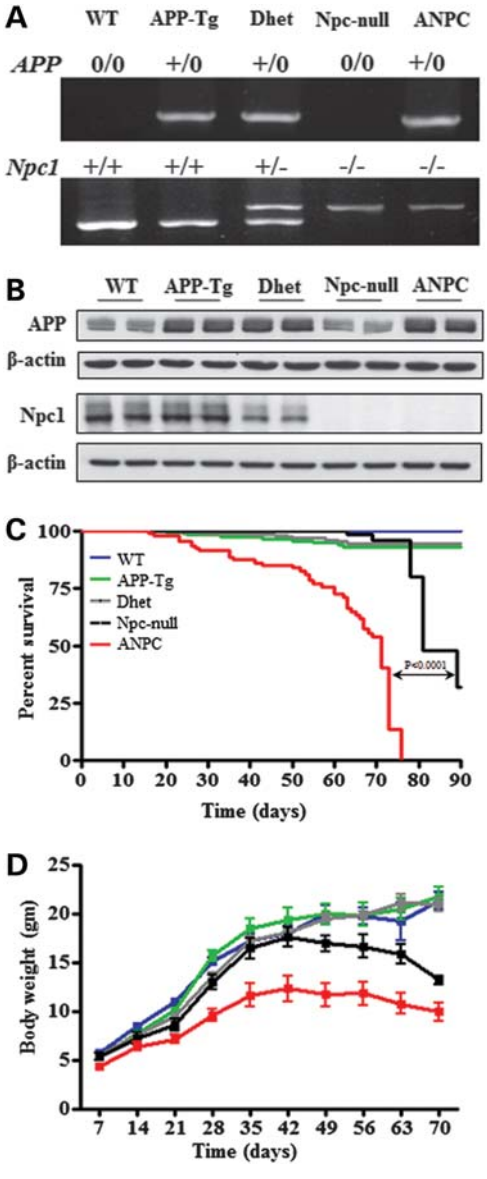

Figure 1. (**A**) PCR analysis of tail biopsy DNA from WT (lane 1), APP-Tg (lane 2), Dhet (lane 3), Npc-null (lane 4) and ANPC (lane 5) mice for human *APP* transgene (upper panel) and mouse *Npc1* gene (lower panel). In *APP* PCR, the presence of a band indicates the presence of the transgene, while its absence indicates lack of the human transgene. For *Npc1* PCR, the presence of the lower band indicates the WT allele and the upper band indicates the knocked-out allele. (**B**) Immunoblotting showing profiles of APP and Npc1 expression in different genotypes as detected with APP C-terminal (Y188) antibody reactive against mouse and human APP (upper panel) and C-terminal Npc1 antibody (lower panel), respectively. The APP-Tg, Dhet and ANPC mice, as expected, exhibit higher levels of APP expression over WT and Npc-null mice harboring only the mouse APP holoprotein. Immunoblotting with the Npc1 antibody revealed the presence of normal levels of Npc1 protein in WT and APP-Tg mice, ~50% of the normal levels in Dhet mice and its absence in ANPC and Npc-null mice. Anti-β-actin antibody was used to monitor an equal loading of proteins. (**C**) Percent survival curves (Kaplan–Meier survival analysis) of different genotypes (WT = 205, APP-Tg = 186, Dhet = 198, Npc-null = 126 and ANPC = 106 animals) showing that ANPC mice have a significantly ($P < 0.0001$) reduced survival compared with mice of other genotypes. (**D**) Weight curves for WT, APP-Tg, Dhet, Npc-null and ANPC assessed between 7 and 70 days of age. ANPC mice show a significantly reduced body weight compared with other genotypes.

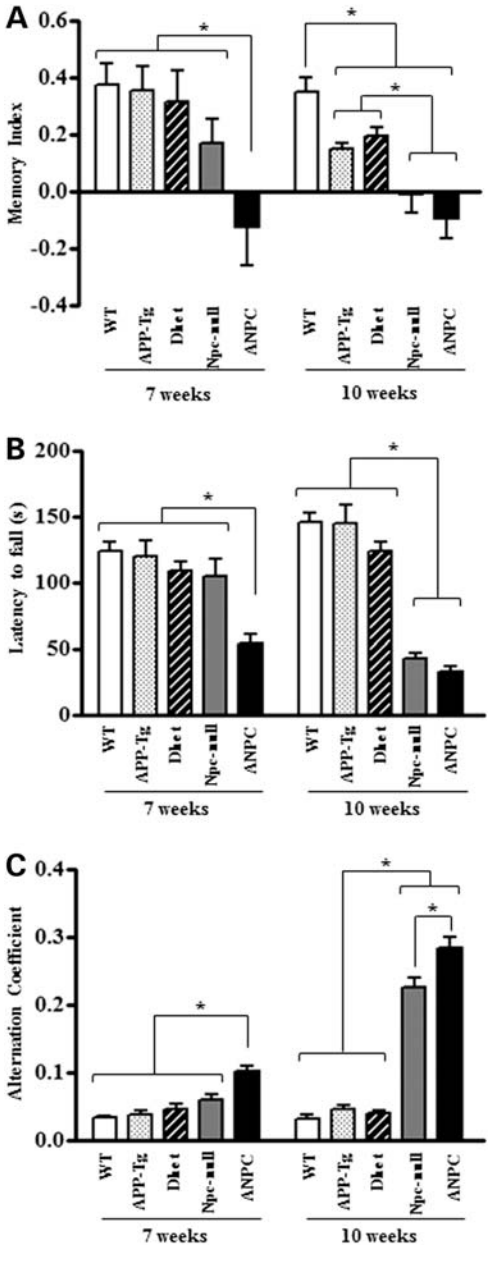

Figure 2. (**A–C**) Cognitive and motor behavioral analysis at 7 and 10 weeks of age in WT, APP-Tg, Dhet, Npc-null and ANPC mice. (A) ANPC mice exhibit a profound deficit in the 3-h object recognition memory test at 7 and 10 weeks of age, whereas the APP-Tg, Dhet and Npc-null mice show a significant deficit only at 10 weeks of age. The values are expressed as means ± SEM of MI scores, with $n = 6–10$ for each genotype. (B) Histograms showing the average latency to fall from an accelerating rotarod for WT, APP-Tg, Dhet, Npc-null and ANPC mice at 7 and 10 weeks of age. ANPC mice exhibited significant motor impairment at 7 weeks, which progressively worsened by 10 weeks. Npc-null mice exhibited significant motor impairment only at 10 weeks, whereas APP-Tg and Dhet mice did not display any impairment at either 7 or 10 weeks of age. Data are expressed as means ± SEM of all trials performed on the final test day, with $n = 6–10$ for each genotype. (C) Histograms showing alternation coefficients representing gait asymmetry in all five genotypes of mice as assessed by measurement of the right hind paw stride length. The WT, APP-Tg and Dhet mice exhibited a normal alternating gait at both 7 and 10 weeks of age. The ANPC mice showed severe gait abnormalities at 7 and 10 weeks of age, whereas Npc-null mice displayed gait disturbances only at 10 weeks. Data are expressed as means ± SEM of alternation coefficients, with $n = 6–10$ for each genotype. $^*P < 0.05$.

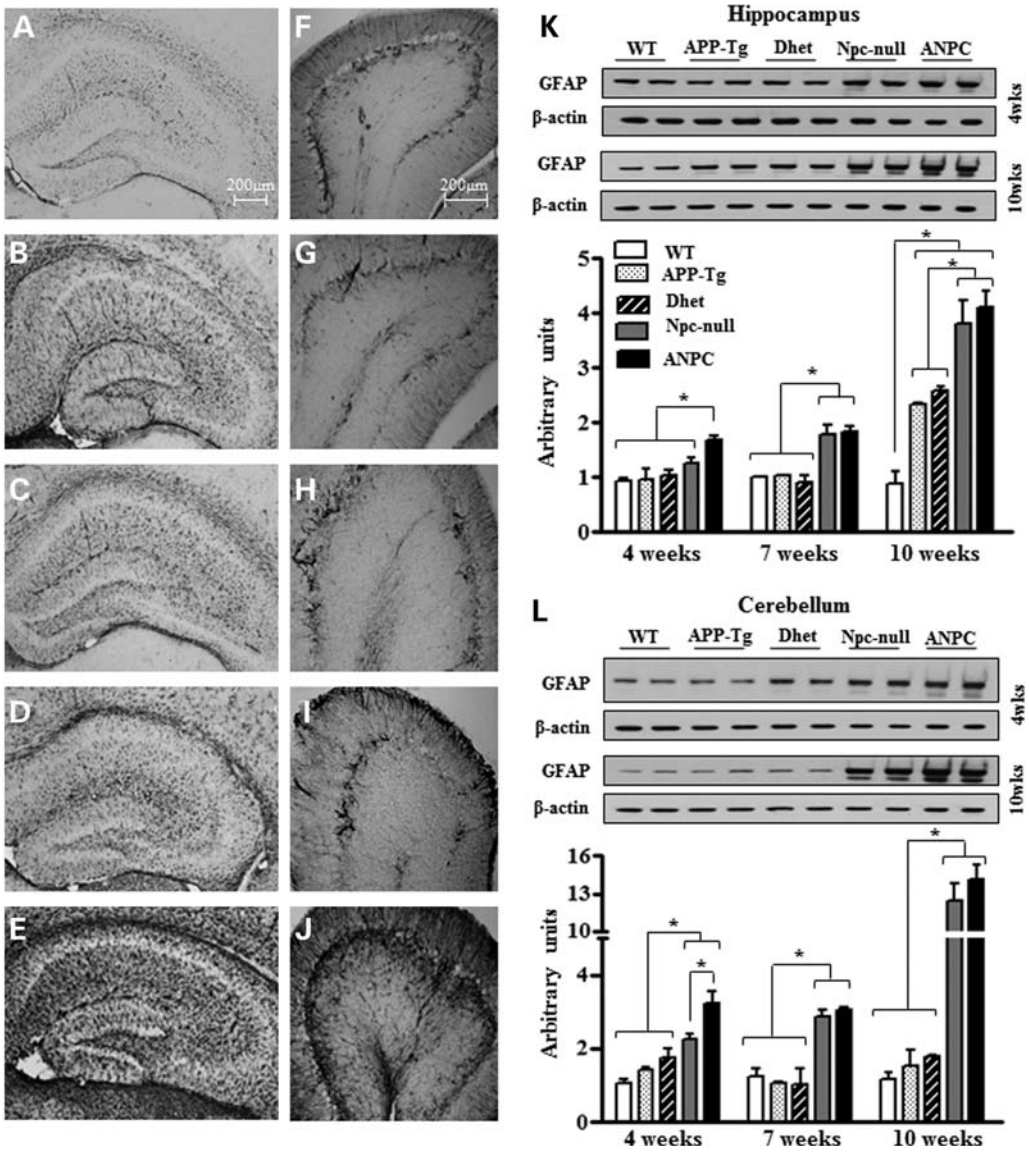

Figure 3. (**A–J**) Bright-field photomicrographs showing GFAP-positive astrocytes in the hippocampus (A–E) and cerebellum (F–J) of 4-week-old WT (A, F), APP-Tg (B, G), Dhet (C, H), Npc-null (D, I) and ANPC (E, J) mice. Note the relative increase in the intensity of GFAP immunoreactivity in the hippocampus and cerebellum of ANPC compared with other genotypes. (**K–L**) Immunoblots and respective histograms showing GFAP levels in the hippocampus (K) and cerebellum (L) of 4-, 7- and 10-week-old WT, APP-Tg, Dhet, Npc-null and ANPC mice. Protein levels were normalized to β-actin. Note the relative increase in the hippocampal and cerebellar GFAP levels in ANPC mice over other genotypes at different age groups. The values are expressed as means ± SEM; $n = 4–6$ animals per genotype and age group. $^{*}P < 0.05$.

(Supplementary Material, Fig. S1A–C). No significant variation was apparent in the sensorimotor behavior between the genotypes at 4 weeks of age (data not shown). The ANPC mice exhibited significantly reduced locomotor activity and increased periods of inactivity in our open-field tests at both 7 and 10 weeks age, whereas Npc-null mice showed these deficits mostly at the later age of 10 weeks only. The APP-Tg and Dhet mice did not show any difference from WT at any age (Supplementary Material, Fig. S1A–C). Furthermore, rotarod performance and gait coordination analysis revealed that motor coordination in Npc-null mice was impaired at 10 weeks but not at 4 or 7 weeks of age. The ANPC mice, on the other hand, displayed a significant impairment in their motor function at 7 weeks, which was further exacerbated by 10 weeks. The APP-Tg and Dhet mice did not show any motor deficit compared with WT mice at any age (Fig. 2B and C).

Intracellular accumulation of unesterified cholesterol

We assessed intracellular cholesterol accumulation across the genotypes by filipin staining which binds unesterified cholesterol (Supplementary Material, Fig. S2A–J). Filipin-labeled cholesterol was evident in almost all neurons of the hippocampus and cerebellum in Npc-null (Supplementary Material, Fig. S2D and I) and ANPC (Supplementary Material, Fig. S2E and J) mice at 4, 7 and 10 weeks of age. By contrast, no cholesterol accumulation was evident in WT, APP-Tg or

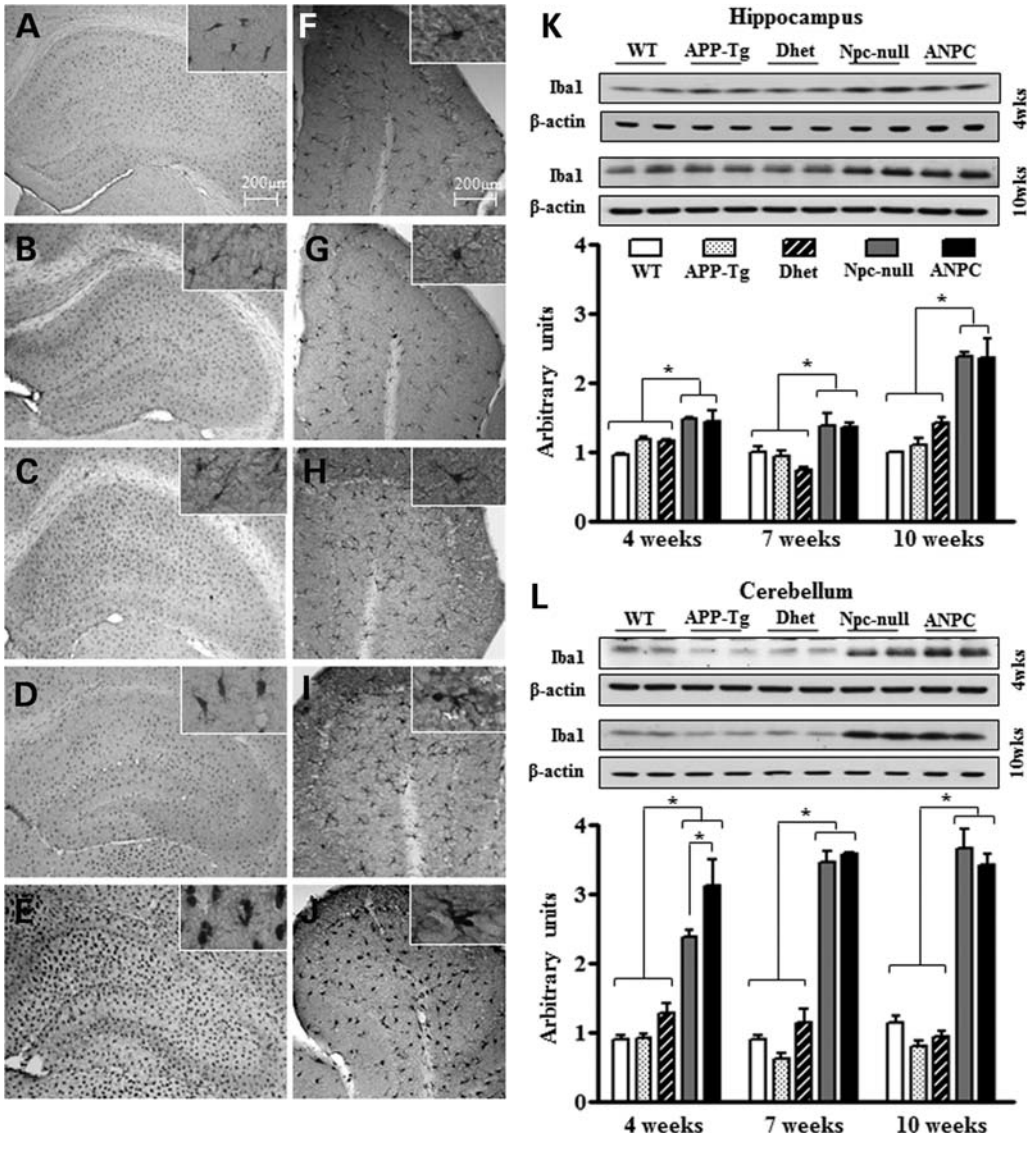

Figure 4. (**A–J**) Bright-field photomicrographs showing Iba1-positive microglia in the hippocampus (A–E) and cerebellum (F–J) of 4-week-old WT (A, F), APP-Tg (B, G), Dhet (C, H), Npc-null (D, I) and ANPC (E, J) mice. Note the relative change in the intensity and morphology of microglia in the hippocampus and cerebellum of ANPC compared with other genotypes. (**K–L**) Immunoblots and respective histograms showing Iba1 levels in the hippocampus (K) and cerebellum (L) of 4-, 7-, and 10-week-old WT, APP-Tg, Dhet, Npc-null and ANPC mice. Protein levels were normalized to β-actin. Note the relative increase in the hippocampal and cerebellar Iba1 levels in ANPC mice over other genotypes at different age groups. The values are expressed as means ± SEM; $n = 4–6$ animals per genotype and age group. $^{*}P < 0.05$.

Dhet littermates at any age group (Supplementary Material, Fig. S2A–H). Interestingly, total cholesterol content in the hippocampus and cerebellum of ANPC and Npc-null mice at 4, 7 and 10 weeks of age, as detected by gas–liquid chromatography, did not exhibit any alteration compared with age-matched WT, APP-Tg or Dhet mice (Supplementary Material, Fig. S2K–M).

Aggravated glial activation and demyelination

At the cellular level, ANPC mice showed a profound increase in the number and activation of glial fibrillary acidic protein (GFAP)-labeled astrocytes in both the hippocampus and cerebellum compared with WT, APP-Tg, Dhet and Npc-null mice (Fig. 3A–J). Our western blot analysis also revealed a significant increase in GFAP levels in the hippocampus and cerebellum of 4, 7 and 10 weeks old ANPC mice compared with WT, APP-Tg and Dhet mice (Fig. 3K and L). The Npc-null mice displayed a significant increase in GFAP levels over the WT, APP-Tg and Dhet mice, mostly at later stages. The relative increase in ANPC over Npc-null mice was evident at 4 weeks but not at later stages.

Consistent with the alteration in astrocytes, ANPC mice showed profound microglial activation in both the hippocampus and cerebellum compared with all other genotypes (Fig. 4A–L). At the cellular levels, ionizing calcium-binding adaptor molecule 1 (Iba1)-labeled microglial cells in WT, APP-Tg and Dhet mouse brains displayed small cell bodies

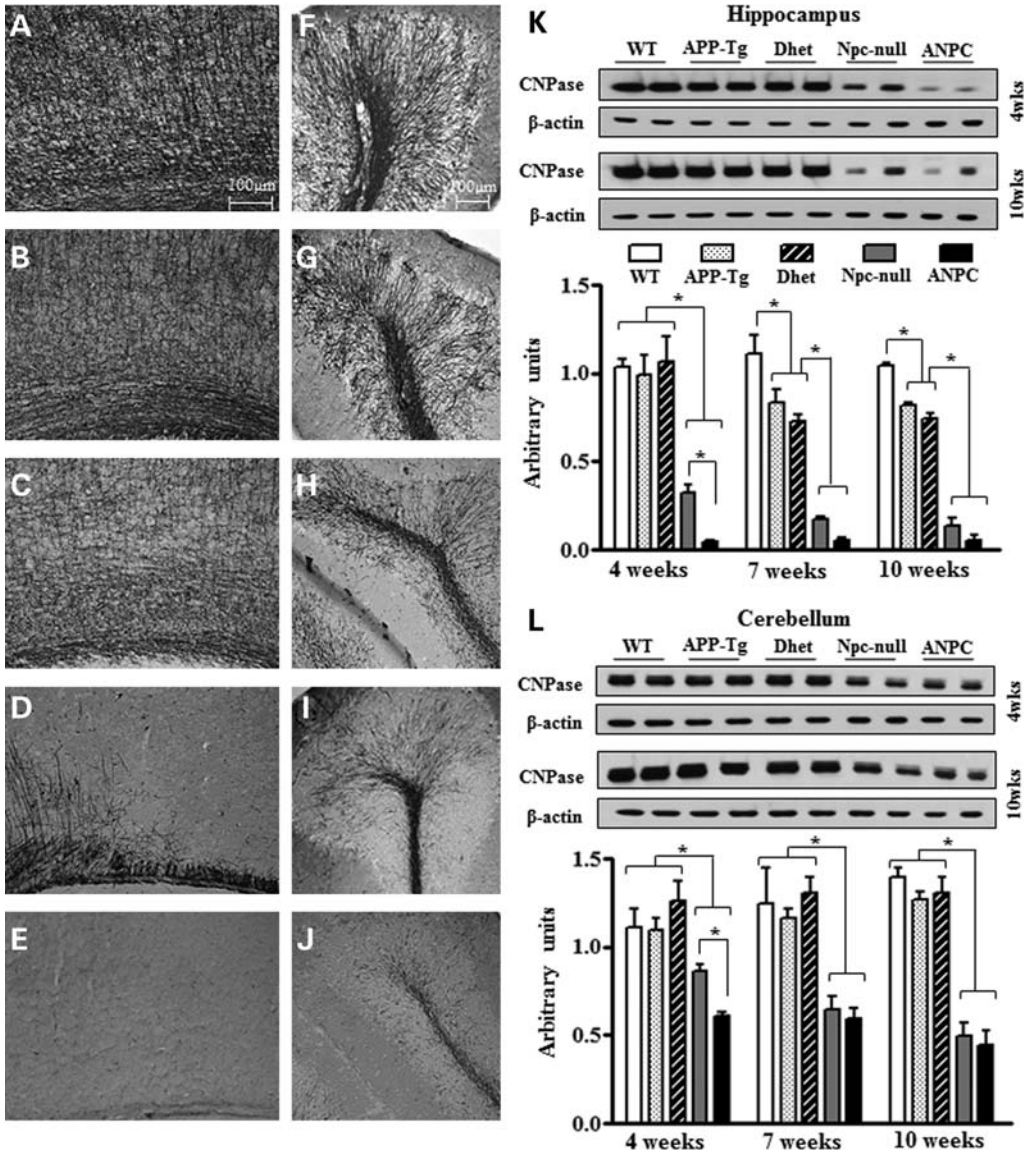

Figure 5. (**A–J**) Bright-field photomicrographs showing 2',3'-cyclic nucleotide 3'-phosphodiesterase (CNPase)-positive oligodendrocytes in the hippocampus/cortex (A–E) and cerebellum (F-J) of 4-week-old WT (A, F), APP-Tg (B, G), Dhet (C, H), Npc-null (D, I) and ANPC (E, J) mice. Note the relative decrease in the intensity of CNPase immunoreactivity in the hippocampus/cortex and cerebellum of ANPC compared with WT, APP-Tg, Dhet and Npc-null mouse brains. (**K–L**) Immunoblots and respective histograms showing CNPase levels in the hippocampus (K) and cerebellum (L) of 4-, 7-, and 10-week-old WT, APP-Tg, Dhet, Npc-null and ANPC mice. Protein levels were normalized to β-actin. Note the relative decrease in the CNPase levels in the hippocampus/cortex and cerebellum of ANPC mice compared with other genotypes at different age groups. The values are expressed as means ± SEM; $n = 4–6$ animals per genotype and age group. $^*P < 0.05$.

with few ramified processes typical of resident microglia (Fig. 4A–C, F–H). In contrast, the ANPC mice showed numerous intensely stained phagocytic, amoeboid microglia microglia were apparent in the cerebellum (Fig. 4E and J). Age-matched Npc-null mice, on the other hand, revealed less activated microglia in both the hippocampus and cerebellum than those observed in ANPC mice (Fig. 4D and I). Our western blot analysis also showed a significant increase in Iba1 levels in the hippocampus and cerebellum of 4, 7 and 10 week old ANPC mice compared with WT, APP-Tg and Dhet mice (Fig. 4K and L). The increase over the Npc-null mice was evident only in 4 weeks cerebellum. Interestingly, the relative increase in Iba1 levels was found to be more profound in the cerebellum than the hippocampus of ANPC and Npc-null mice compared with the other lines of mice.

Immunohistochemical staining with the oligodendrocyte marker 2',3'-cyclic nucleotide 3'-phosphodiesterase (CNPase) showed a dramatic loss of myelin fibre tracts in the ANPC hippocampus/cortex and cerebellum compared with the other lines of mice (Fig. 5A–J). This was substantiated by our western blot data, showing striking decreases in CNPase levels in ANPC hippocampus and cerebellum at 4, 7 and 10 weeks (Fig. 5K and L). Npc-null mice, as reported earlier (38), also showed significant demyelination at various ages, but this was found to be less severe than ANPC mice at earlier stages. Additionally, the levels of CNPase in the hippocampus, but not in the cerebellum,

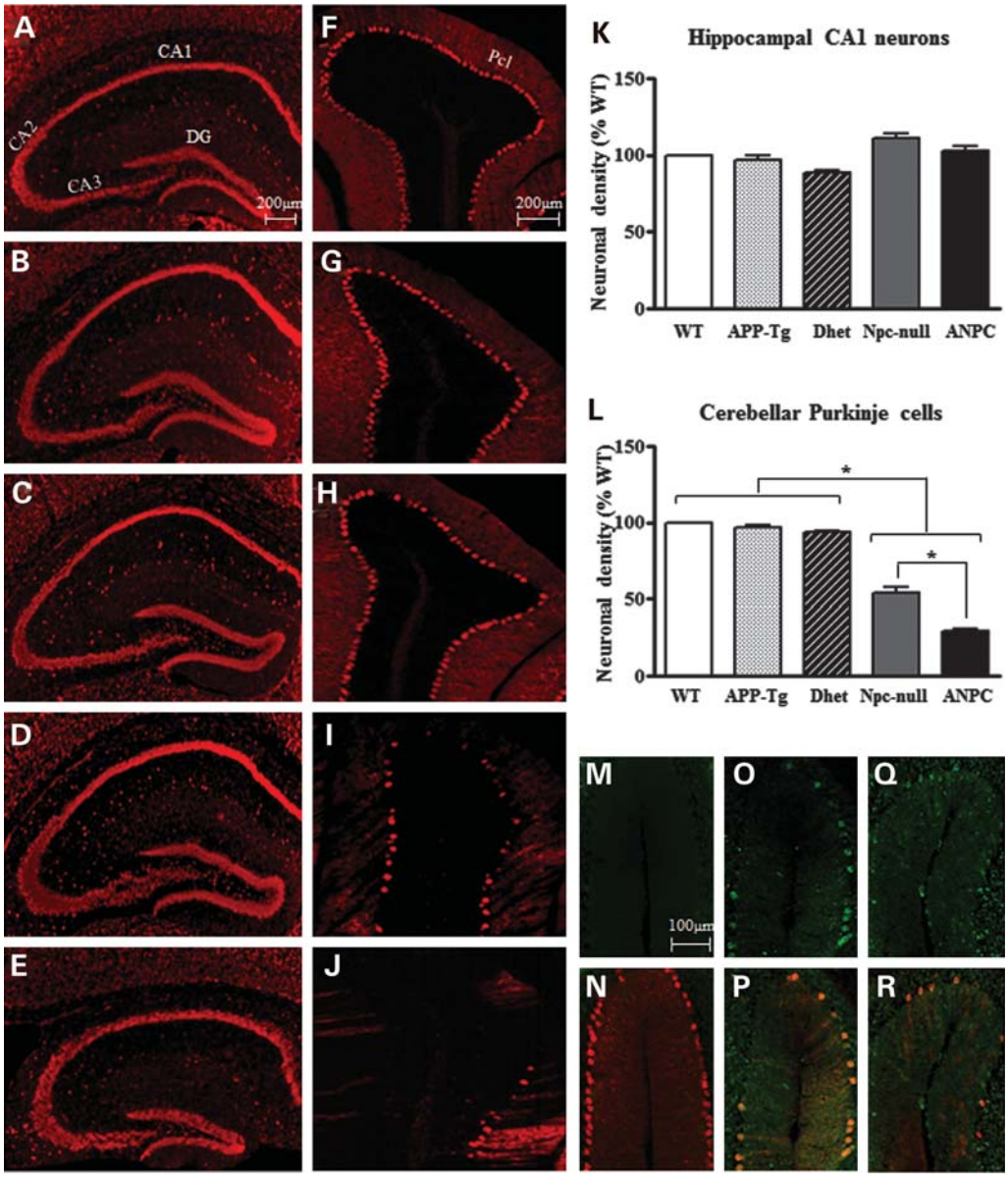

Figure 6. (**A–E**) Photomicrographs showing NeuroTrace-labeled hippocampal sections from mice of different genotypes at 7 weeks of age. No apparent loss of neurons was evident in the hippocampus of ANPC (E) compared with WT (A), APP-Tg (B), Dhet (C) and Npc-null (D) littermates. (**F–J**) Photomicrographs showing a calbindin-positive cerebellar Purkinje cell layer (Pcl) from 7-week-old mice of different genotypes. Note the relative loss of Purkinje cells in Npc-null (I) and ANPC (J) mice compared with WT (F), APP-Tg (G) and Dhet (H) mice. (**K–L**) Quantitative analysis of neuronal density in the hippocampal CA1 region (K) and cerebellar Pcl (L) of APP-Tg, Dhet, Npc-null and ANPC brains expressed as percentage of WT. Note the significant loss of cerebellar Purkinje cells (L) but no alteration in the hippocampal neurons (K) in Npc-null and ANPC mice compared with the other genotypes. The magnitude of Purkinje cell loss was more profound in ANPC than in age-matched Npc-null mice. (**M–R**) Photomicrographs showing co-localization of cleaved caspase-3 (green) with calbindin-positive (red) Purkinje cells in WT, Npc-null and ANPC cerebellum. M, O and Q represent the cleaved caspase-3 labeling in WT, Npc-null and ANPC, respectively, while N, P, R are the merged images. CA1-CA3, Cornu Ammonis 1–3; DG, Dentate Gyrus. The values are expressed as means ± SEM. $^{*}P < 0.001$.

were depleted in APP-Tg and Dhet mice at later stages compared with age-matched WT mice (Fig. 5K and L).

Loss of neurons and synaptic markers

Our APP-Tg mice, as reported for most other lines of mutant APP mice, do not exhibit frank loss of neurons in any brain region (28,29). The Npc-null mice, on the other hand, show a progressive loss of neurons in selected brain regions such as thalamus and cerebellum but not in the hippocampus (5,6). In keeping with these results, we observed a significant decrease in the number of cerebellar Purkinje cells in ANPC and Npc-null mice compared with WT, APP-Tg and Dhet mice (Fig. 6A–L). The magnitude of cell loss was found to be more pronounced in ANPC than in the Npc-null mice (Fig. 6L). Labeling of degenerating neurons with cleaved caspase-3 suggested the possible involvement of apoptosis in triggering the loss of neurons (Fig. 6M–R). The hippocampus, on the other hand, did not exhibit any significant neuronal loss either in APP-Tg, Dhet, ANPC or Npc-null mice compared

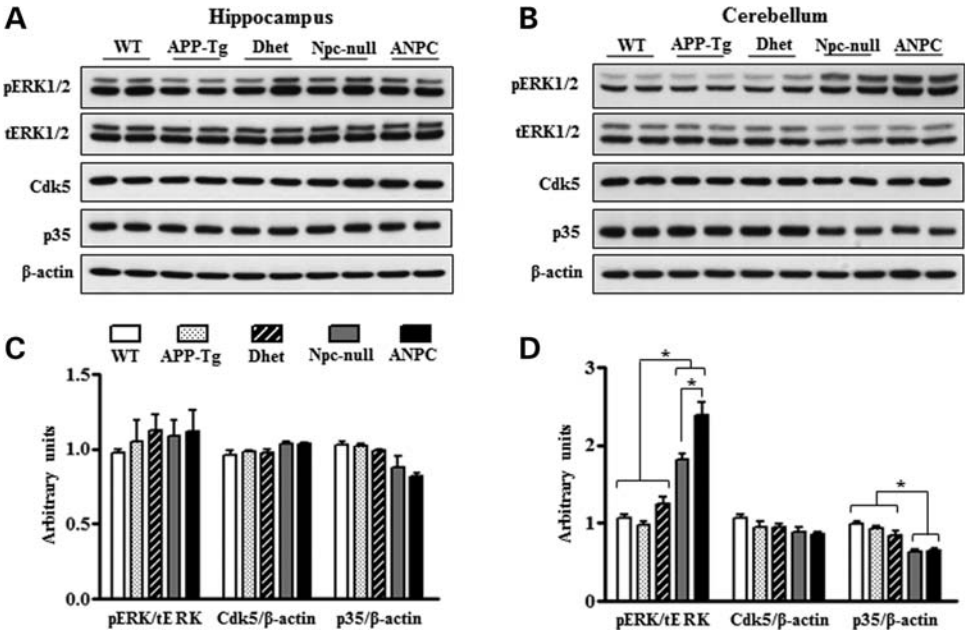

Figure 7. (**A–D**) Immunoblot analysis of tau kinases in the hippocampus (A, C) and cerebellum (B, D) of 7-week-old WT, APP-Tg, Dhet, Npc-null and ANPC mice. Phospho-ERK1/2 levels were significantly increased in the cerebellum (B, D) but not in the hippocampus (A, C) of ANPC mice compared with other genotypes. The cerebellum of Npc-null mice also showed a significant increase in phospho-ERK1/2 levels compared with other genotypes but is less pronounced than ANPC mice (B, D). Quantitative analysis of Cdk5 levels normalized to β-actin showed no significant alteration between the genotypes either in the hippocampal (A, C) or in the cerebellar (B, D) brain regions. Immunoblotting using p35 antibody indicates a decrease in p35 levels in the cerebellum of ANPC and Npc-null mice relative to WT, APP-Tg and Dhet mice (B, D). No alteration in p35 levels was observed in the hippocampus between the genotypes (A, C). The values are expressed as means ± SEM; $n = 4–6$ animals per genotype. $^{*}P < 0.05$.

with WT mice (Fig. 6A–E, K). The levels of presynaptic marker synaptophysin and postsynaptic marker postsynaptic density protein 95 (PSD95) were markedly decreased in 7- and/or 10-week-old Npc-null and ANPC cerebellum compared with WT, APP-Tg and Dhet mice. In the hippocampus, however, no alteration in synaptophysin level was evident at any age, whereas the level of PSD95 was decreased in 10-week-old Npc-null and ANPC mice compared with other lines (Supplementary Material, Fig. S3A–D).

Activation of tau kinases and phosphorylation of tau

Although florid tau pathology is not apparent in either APP-Tg or Npc-null mice, there is evidence that altered cholesterol levels can regulate tau phosphorylation under *in vitro* conditions (39). To determine whether overexpression of APP together with intracellular cholesterol accumulation can influence tau phosphorylation under *in vivo* paradigm, we first evaluated tau kinases in all lines of mice. Our results clearly demonstrated a significant up-regulation of phospho-extracellular signal-regulated kinase 1/2 (ERK1/2) in the cerebellum, but not in the hippocampus, of Npc-null or ANPC mice (Fig. 7A–D). Additionally, the steady-state levels of p35 were found to be decreased in the cerebellum, but not hippocampus, of Npc-null and ANPC mice compared with other lines of mice (Fig. 7A–D). In contrast, the levels of phospho-glycogen synthase kinase-3β (GSK-3β) did not alter in the ANPC or Npc-null mice (Supplementary Material, Fig. S4A and B). As a follow-up, we measured the levels of total tau using Tau-1 and Tau-5 antibodies and phospho-tau using various epitope specific antibodies in the hippocampus and cerebellum of five different lines of mice (Fig. 8A–D). Our results clearly showed that the total-tau level was strikingly decreased in the cerebellum, but not hippocampus, of ANPC and Npc-null mice compared with other lines. Interestingly, the levels of phospho-tau remain unaltered in both brain regions of ANPC and Npc-null mice with respect to other genotypes. Thus, it is evident that phosphorylation of tau is selectively increased in the affected cerebellar region, which was more pronounced in ANPC than Npc-null mice. More recently, a number of studies have indicated that proteolytic cleavage of tau protein, in addition to enhanced phosphorylation, may have a role in the degeneration of neurons (40–42). Our results showed that levels of caspase-cleaved tau are markedly increased in the cerebellum, but not hippocampus, of the ANPC and Npc-null mice (Fig. 8A–D). The relative change, however, was more obvious in ANPC than Npc-null mice. At the cellular level, cleaved tau immunoreactivity was evident only in the Purkinje cells of the ANPC and Npc-null mice but not in WT, APP-Tg or Dhet mice (Fig. 8E–G).

Increased activity and cytosolic levels of cathepsin D

Several studies have shown that up-regulation of lysosomal enzymes within lysosomes can prevent sub-lethal damage (43), whereas lysosomal rupture leading to sustained release of enzymes into the cytosol can induce cell death via cytochrome c release from mitochondria (44–46). To determine the potential involvement of the lysosomal enzymes in ANPC mice, we measured the level/activity and subcellular distribution of cathepsin D in all five lines of mice (Fig. 9A–F;

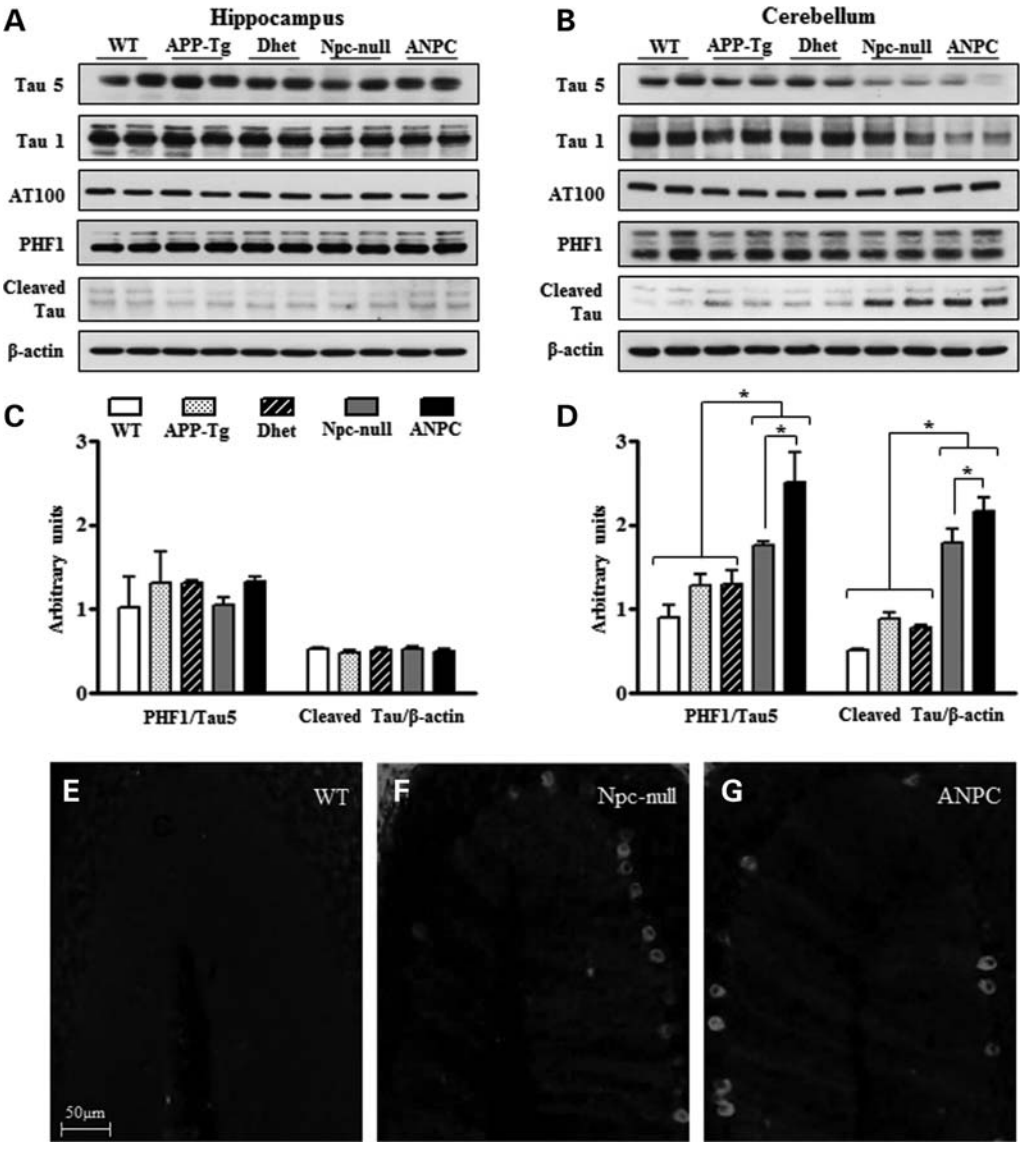

Figure 8. (**A**–**D**) Immunoblot analysis of total, phospho and cleaved tau levels in the hippocampus (A, C) and cerebellum (B, D) of 7-week-old WT, APP-Tg, Dhet, Npc-null and ANPC mice. Total tau was detected by Tau-5 (phospho-independent anti-tau antibody) and Tau-1 (dephosphorylated tau at serines 195, 198, 199 and 202) antibodies, whereas phospho-tau was detected using AT 100 (T212, S214 and T217) and PHF1 (S396/S404) antibodies. Note the decrease in total-tau levels in the cerebellum (B) but not in the hippocampus (A) of Npc-null and ANPC mice compared with WT, APP-Tg and Dhet mice. Quantitative analysis of phospho-tau levels normalized to total tau showed hyperphosphorylation of tau protein specifically in the cerebellum of Npc-null and ANPC mice compared with other genotypes (C, D). The increased level of phospho-tau was more pronounced in the ANPC than Npc-null mice. The caspase-cleaved tau level showed marked increase in the cerebellum (B, D) but not in the hippocampus (A, C) of Npc-null and ANPC mice than WT, APP-Tg and Dhet mice. The alteration in the levels of cleaved tau was found to be more pronounced in ANPC mice than Npc-null mice. (**E**–**G**) Representative images from WT (E), Npc-null (F) and ANPC (G) cerebellar sections showing immunolabeling for cleaved Tau antibody. The values are expressed as means ± SEM; $n = 4–6$ animals per genotype. $^{*}P < 0.05$.

Supplementary Material, Fig. S5A and B). Our results clearly showed that cathepsin D levels and activity were significantly higher in the hippocampus and even more pronounced in the cerebellum of ANPC and Npc-null mice compared with other lines of mice (Fig. 9A–D). It is of interest to note that the activity of this enzyme was found to be increased more profoundly in ANPC cerebellum compared with Npc-null mice (Fig. 9D). Our subcellular fractionation results further revealed that cytosolic cathepsin D levels were higher in the cerebellum of ANPC and Npc-null mice compared with WT mice (Fig. 9F). Similar to cathepsin D, the levels of cytochrome c and Bcl-2-associated X protein (Bax), but not apoptosis inducing factor (AIF), were increased in the cerebellar cytosolic fraction of ANPC and Npc-null mice compared with other lines (Fig. 9F, Supplementary Material, Fig. S5B). The relative change was found to be more obvious in the ANPC than Npc-null mice (Fig. 9F). In contrast to the cerebellum, alterations in hippocampal cytosolic cathepsin D, cytochrome c and Bax levels were less apparent in ANPC and Npc-null mice compared with WT mice (Fig. 9E, Supplementary Material, Fig. S5A). It is also of interest

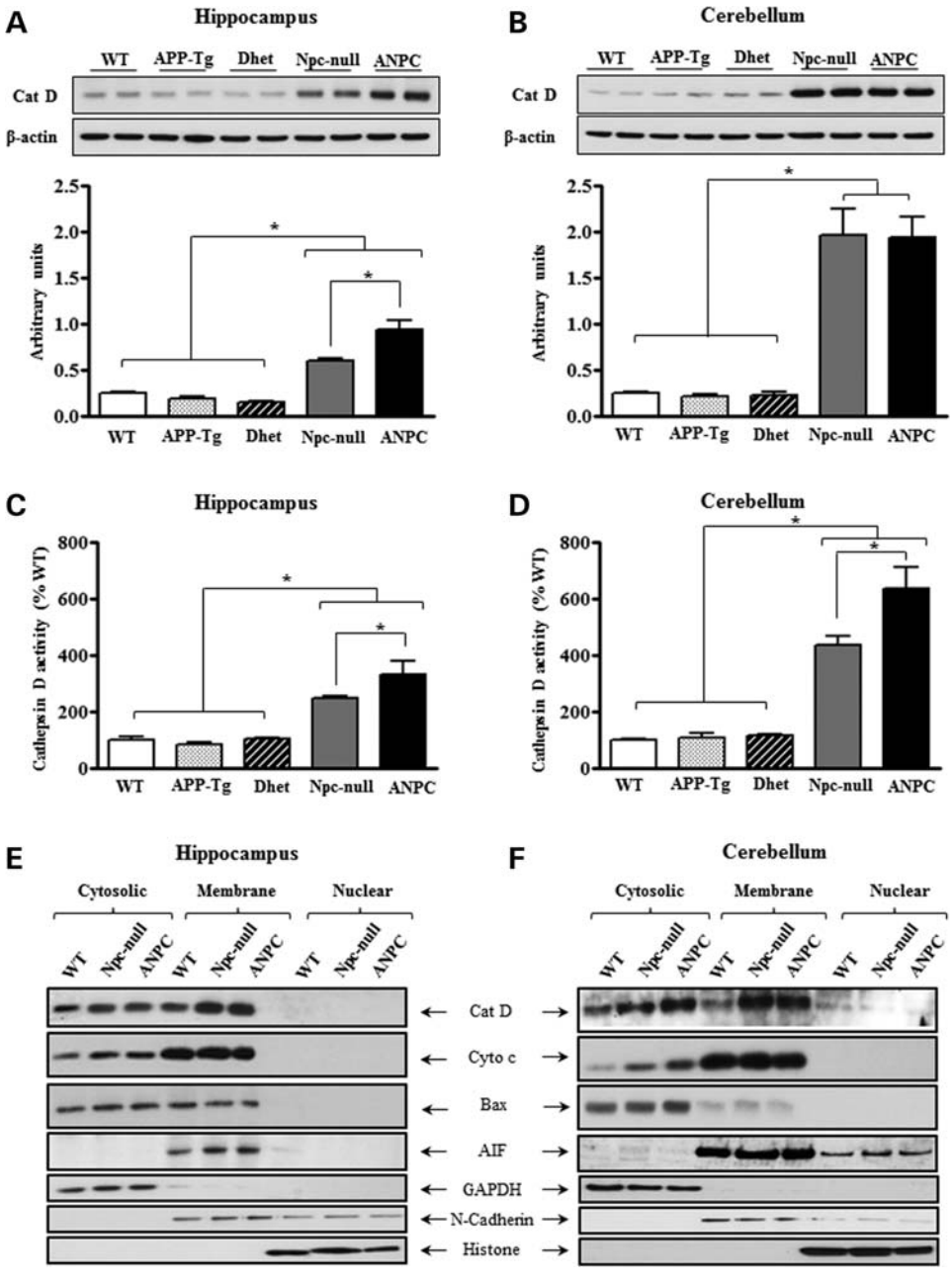

Figure 9. (**A**–**B**) Immunoblots and respective histograms showing increased mature Cat D levels in the hippocampus (A) and cerebellum (B) of 7-week-old ANPC and Npc-null mice compared with age-matched WT, APP-Tg and Dhet mice. Note the relatively greater fold increase in Cat D levels in the cerebellum than the hippocampus of ANPC and Npc-null mice compared with other genotypes. Protein levels were normalized to β-actin. (**C**–**D**) Histograms showing Cat D enzyme activity in the hippocampus (C) and cerebellum (D) of 7-week-old APP-Tg, Dhet, Npc-null and ANPC mice expressed as a percentage of activity in WT. Note the relatively greater increase in Cat D activity in the hippocampus and cerebellum of ANPC mice compared with other genotypes. (**E**–**F**) Representative immunoblots showing a subcellular distribution of Cat D, Cyto c, Bax and AIF in the hippocampus (E) and cerebellum (F) of 7-week-old WT, Npc-null and ANPC mice. Note the relatively higher cytosolic levels of Cat D, Cyto c, and Bax in the cerebellum than the hippocampus of Npc-null and ANPC mice compared with WT. Immunoblots for GAPDH, N-cadherin and Histone 3 represent the loading controls for the cytosolic, membrane and nuclear fractions, respectively. Cat D, cathepsin D; cyto c, cytochrome c; Bax, Bcl-2-associated X ptotein; AIF, apoptosis-inducing factor; GAPDH, glyceraldehyde-3-phosphate dehydrogenase. Histogram values represent means ± SEM; $n = 4–6$ animals per genotype. $^{*}P < 0.05$.

to note that changes observed in the hippocampus did not reveal much variation between ANPC and Npc-null mice as evident in the cerebellum. The cytosolic levels of cathepsin D, cytochrome c and Bax in APP-Tg and Dhet mice did not differ from the WT mice in either brain region (Supplementary Material, Fig. S5A and B).

Effect of 2-HPC treatment

To determine whether lowering cholesterol accumulation can attenuate the aforementioned abnormalities, we injected WT, Npc-null and ANPC mice with 2-HPC or saline at postnatal day 7 and then evaluated their behavioral and pathological

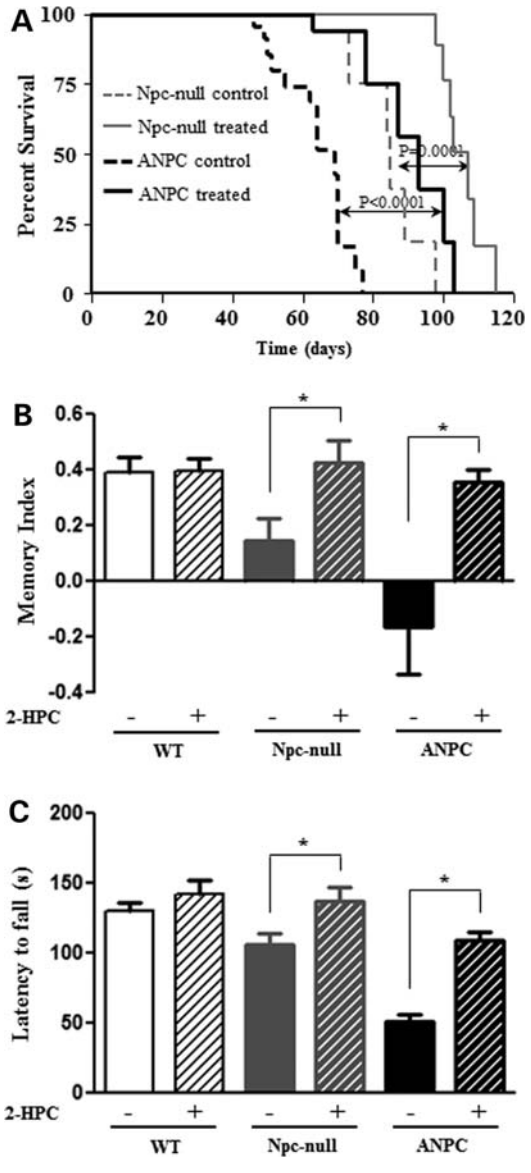

Figure 10. (**A**–**C**) Effect of 2-HPC treatment on survival, cognitive and motor analysis in ANPC and Npc-null mice. (A) Survival curve showing that 2-HPC treatment significantly prolonged the life of both ANPC and Npc-null mice ($P \leq 0.0001$ by log-rank test) compared with saline-treated mice. (B and C) Histograms showing that 2-HPC treatment significantly improved the performance of Npc-null and ANPC mice in 3-h object recognition memory (B) and rotarod (C) tests compared with their respective saline-treated control groups but had no effect on the WT animals. The values are expressed as means ± SEM, with $n = 6$–10 for each group. $^{*}P < 0.05$.

features at 4 or 7 weeks of age. The ANPC and Npc-null mice treated with 2-HPC lived significantly longer than the respective saline-injected mice (ANPC median survival: 103 days versus 69 days; Npc-null median survival: 107 days versus 85 days) (Fig. 10A). Additionally, our results clearly showed that 2-HPC treatment can lead to significant improvement in the motor and cognitive performances of 7-week-old ANPC and Npc-null mice compared with the respective saline-treated genotypes (Fig. 10B and C).

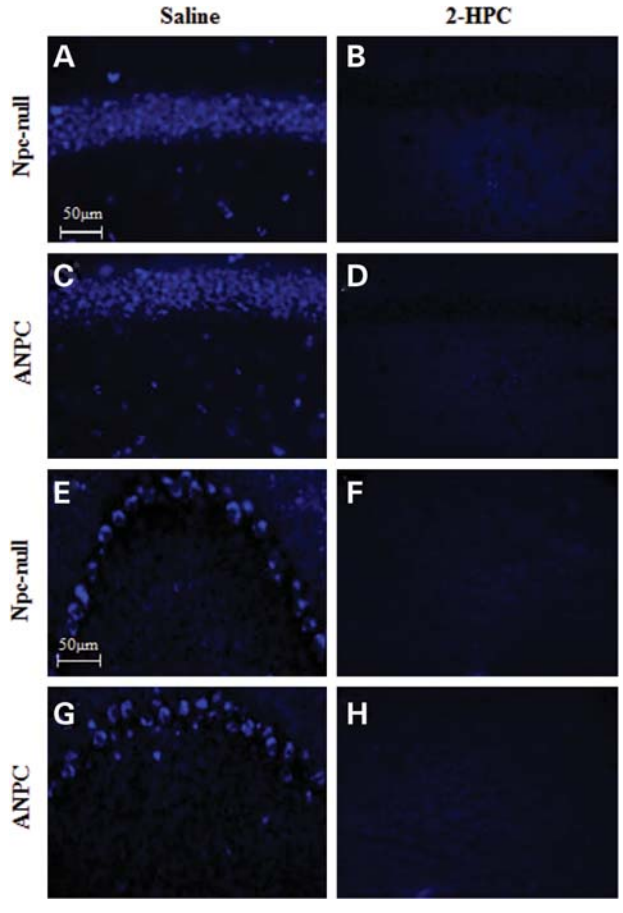

Figure 11. (**A**–**H**) Effect of 2-HPC treatment on cholesterol accumulation in Npc-null and ANPC mice. Filipin labeling in the hippocampal (A, B, C, D) and cerebellar (E, F, G, H) brain sections of Npc-null (A, B, E, F) and ANPC (C, D, G, H) mice revealed no apparent cholesterol accumulation in 2-HPC-treated mice compared to saline-treated control mice. $n = 3$–4 animals per treatment group.

At the cellular level, we observed that 2-HPC treatment was able to sequester filipin-labeled cholesterol accumulation in most neurons in 4-week old ANPC and Npc-null mice (Fig. 11A–H). Accompanying these changes, the number of surviving Purkinje cells in treated ANPC and Npc-null mice, *albeit* significantly lower than WT mice, was found to be doubled compared with the saline-injected ANPC and Npc-null mice (Fig. 12A–E). Our immunohistochemical analysis further showed a significant decrease in the activation of GFAP-labeled astrocytes and Iba1-labeled microglia in both the hippocampus and cerebellum of 2-HPC-treated ANPC and Npc-null mice compared with the respective saline-treated animals (Fig. 13A–P). The beneficial effects of 2-HPC were also reflected with a substantial increase in CNPase immunoreactivity, suggesting preservation of brain myelination (Fig. 13Q–X). More interestingly, 2-HPC treatment, as evident from our western blot analysis, markedly attenuated the enhanced levels of phospho-ERK1/2 in the cerebellum of ANPC and Npc-null mice (Fig. 14A and B). This was accompanied by a parallel increase in total-tau and a decrease in cleaved tau levels in the cerebellum of 2-HPC-treated ANPC and Npc-null animals compared with the respective saline-injected genotypes (Fig. 15A and B).

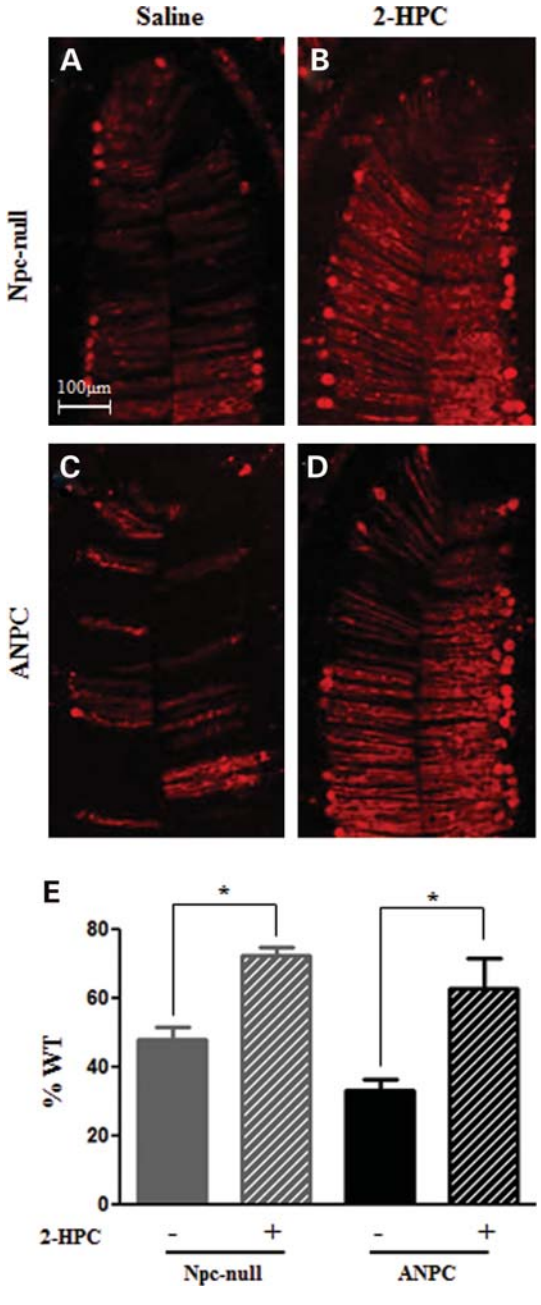

Figure 12. (**A**–**E**) Photomicrographs and histograms showing the effect of 2-HPC treatment on the cerebellar Purkinje cell viability in Npc-null and ANPC mice. (A–D) Representative cerebellar sections from 7-week-old saline- (A, C) and 2-HPC- (B, D) treated Npc-null (A, B) and ANPC (C, D) mice showing a calbindin-positive Purkinje cell layer. (E) Quantitative analysis revealed a significant increase in the survival of cerebellar Purkinje cells in 2-HPC-treated Npc-null and ANPC mice compared with the respective saline-treated control mice. The values are expressed as means ± SEM, with $n = 3–4$ animals for each group. $^{*}P < 0.05$.

DISCUSSION

Using a new line of bigenic ANPC mice, the present study shows that overexpression of APP in the absence of functional Npc1 protein can significantly decrease longevity, impair motor and object recognition memory functions, exacerbate glial pathology and accelerate degeneration of neurons. This is accompanied by altered function of the EL system and increased phosphorylation and cleavage of tau protein. Neuropathological abnormalities are more profound in the cerebellum, exhibiting a significant loss of neurons than the relatively spared hippocampus in ANPC mice. This is supported by the results which showed that (i) proliferation of astrocytes and microglia and loss of myelin are notably higher in the cerebellum than the hippocampus, (ii) phosphorylation and cleavage of tau protein are selectively enhanced in the cerebellum and (iii) cytosolic levels of cathepsin D, cytochrome c and Bax are increased more predominantly in the cerebellum than the hippocampus. It is also of interest to note that cerebellar dysfunctions in ANPC mice are conspicuously more severe than in Npc-null, Dhet, APP-Tg and WT mice. Reversal of accumulated cholesterol by 2-HPC treatment not only prolongs the lifespan but also attenuates behavioral and glial pathology in ANPC mice. This is accompanied by enhanced survival of neurons and decreased phosphorylation/cleavage of tau protein. Collectively, these results suggest that overexpression of APP in the Npc-null mice can influence longevity as well as a wide spectrum of behavioral and neuronal abnormalities associated with NPC disease, whereas reversal of cholesterol accumulation is beneficial in attenuating these abnormalities.

Multiple lines of evidence have shown that elevated cholesterol levels can influence APP metabolism as well as AD-related pathology (47). Conversely, APP-Tg mice exhibit altered levels of lipids surrounding plaque cores that may have a role in the dynamic of amyloid aggregation (48). The present study clearly reveals that APP overexpression did not elicit any obvious alterations either on intracellular accumulation or total levels of cholesterol in Npc-null mice. This could possibly reflect a compensatory adjustment where increased cholesterol levels in the cell bodies are obscured by its reduction in myelin, the major repository of cholesterol in the central nervous system (26). Overexpression of APP, however, drastically reduces the lifespan of Npc-null mice along with a progressive decline in their body weight. This is interesting in the context of the results, which showed that decreasing *de novo* cholesterol synthesis/turnover by deleting the 24-hydroxylase gene can prolong the lifespan of APP-Tg mice (49). Accompanying the mortality rate, object recognition memory and a spectrum of sensorimotor functions including locomotor activity and gait coordination are impaired earlier in ANPC mice than in Npc-null, APP-Tg, Dhet and WT mice. Given the evidence that all these mice were generated on the same outbred genetic background, the behavioral changes observed in ANPC mice most likely reflect the influence of APP overexpression in the context of an Npc-null genotype, rather than the coincident segregation of (hypothetical) modifier genes. Prior studies have reported motor impairments in the Npc-null mice (37) and object memory deficits in APP-Tg mice without any evidence of motor dysfunction (30). Our results, however, reveal that overexpression of APP induces early motor and object memory deficits in Npc-null mice compared with other littermates. While object memory relies on the integrity of entorhinal-hippocampal circuitry (50), the cerebellum is known to play a critical role in regulating normal motor activity (51,52). The early manifestation of behavioral deficits in ANPC

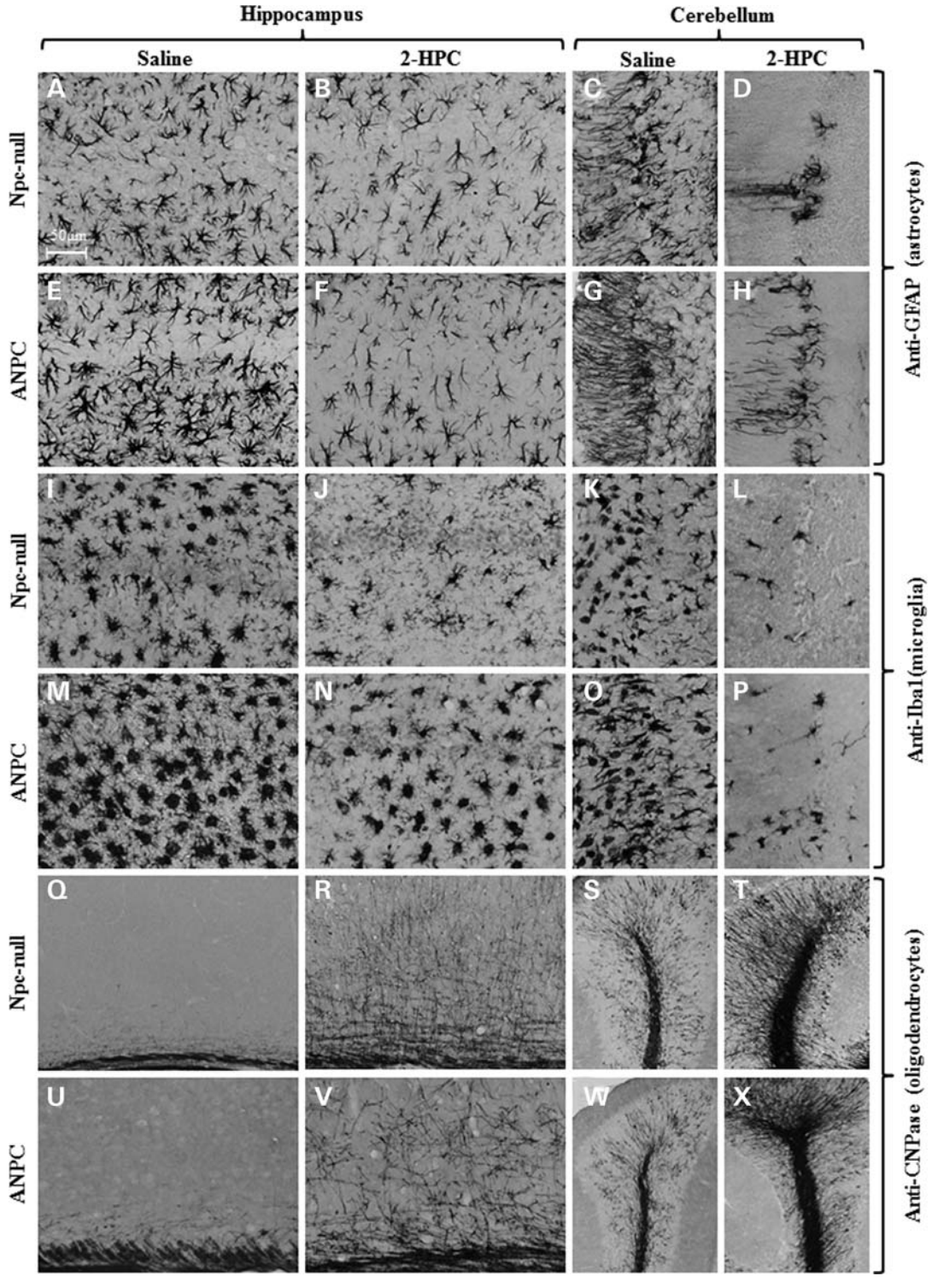

Figure 13. (**A–X**) Photomicrographs showing the effect of 2-HPC treatment on different glial markers in the hippocampus and cerebellum of Npc-null and ANPC mice. Note the attenuation in the proliferation/activation of GFAP-labeled astrocytes (A–H) and Iba1-labeled microglia (I–P) in the hippocampus (A, B, E, F, I, J, M, N) and cerebellum (C, D, G, H, K, L, O, P) of 2-HPC-treated Npc-null (B, D, J, L) and ANPC (F, H, N, P) mice compared with the respective saline-treated control (A, C, E, G, I, K, M, O) mice. The expression of CNPase-immunoreactive oligodendrocytes was found to be increased in the hippocampus (Q, R, U, V) and cerebellum (S, T, W, X) of 2-HPC-treated Npc-null (R, T) and ANPC (V, X) mice compared with respective saline-treated control (Q, S, U, W) mice. $n = 3–4$ animals per treatment group.

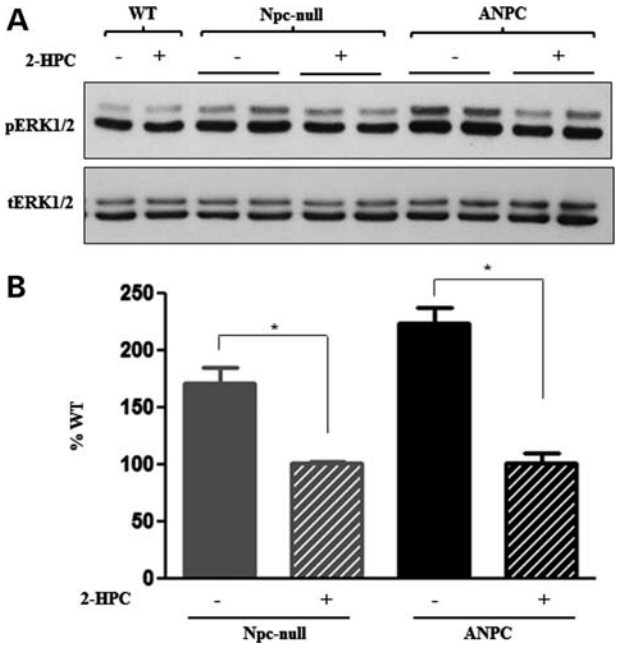

Figure 14. (**A** and **B**) Immunoblot analysis showing the effect of 2-HPC treatment on phospho-ERK1/2 levels in Npc-null and ANPC mice. (A) Representative immunoblots illustrating reversal in the increase of phospho-ERK1/2 levels in 7-week-old Npc-null and ANPC cerebellum following 2-HPC treatment. (B) Quantitative analysis of phospho-ERK1/2 normalized to total ERK levels illustrating significant down-regulation in phosho-ERK1/2 levels in 2-HPC-treated Npc-null and ANPC compared with their respective saline-treated groups. The values are expressed as means ± SEM, with $n = 4$ for each group. $^{*}P < 0.05$.

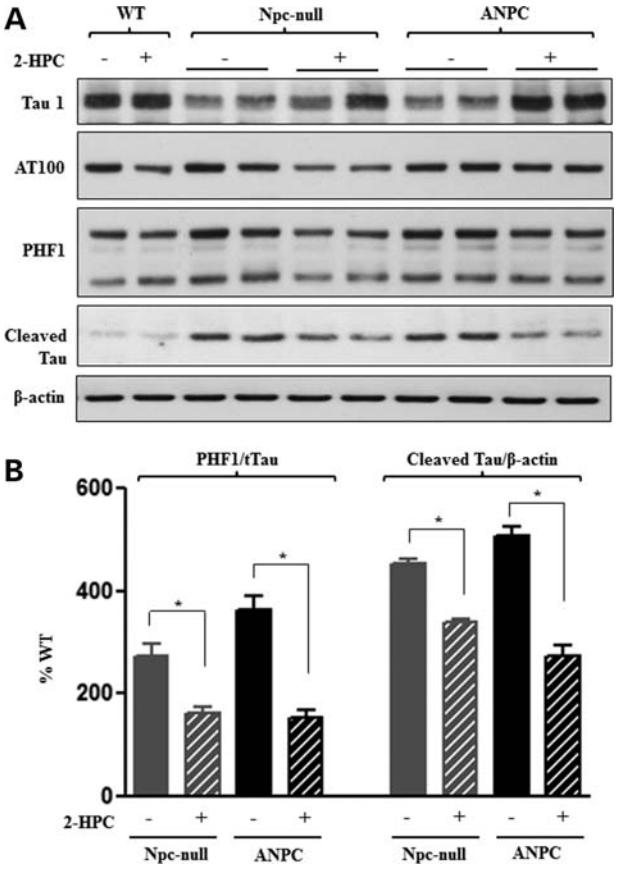

Figure 15. (**A** and **B**) Immunoblot analysis showing the effect of 2-HPC treatment on total, phospho and cleaved tau levels in Npc-null and ANPC mice. (A) Representative immunoblots illustrating reversal in the decrease of total-tau but no alterations in phospho-tau levels in 7 weeks old Npc-null and ANPC cerebellum following 2-HPC treatment. Increased levels of caspase-cleaved tau were also attenuated in 2-HPC-treated Npc-null and ANPC mice compared with their respective saline-treated control mice. (B) Quantitative analysis showing reduced phospho-tau/total-tau ratio and cleaved tau products in the cerebellum of 2-HPC-treated 7-week-old Npc-null and ANPC compared with their respective saline-treated groups. The values are expressed as means ± SEM, with $n = 4$ for each group. $^{*}P < 0.05$.

mice possibly relates to their neuropathological abnormalities that precede those found in Npc-null and APP-Tg mice.

Earlier studies have shown activation of both astrocytes and microglia in APP-Tg and Npc-null mice, but loss of myelin only in Npc-null mice (5,10,53). The overall glial pathology in ANPC mice is markedly exacerbated at the earlier stages compared with other littermates, whereas at the later stages it varies from other genotypes except Npc-null mice. This suggests that APP overexpression may induce early glial activation in Npc-null mice which can subsequently influence disease pathology. This is partly reflected in the loss of cerebellar Purkinje cells which is more severe in ANPC than in Npc-null mice. Interestingly, hippocampal neurons, even though accumulate cholesterol, are found to be relatively spared in ANPC mice as observed in Npc-null mice. It is possible that these neurons are being protected against toxic insults by an up-regulation of survival mechanisms as demonstrated in mutant APP-Tg mice (54) or they might be vulnerable if the animals would have lived longer.

Most APP-Tg mice do not exhibit any overt loss of neurons, but there is evidence that defective steroidogenesis (55), abnormal lipid trafficking (56) and production of inflammatory molecules (10) from glia can negatively affect NPC disease progression and neuronal viability. This is supported by the observation that an astrocyte-targeted Npc1 transgene can enhance lifespan and decrease neurodegeneration in Npc-null mice (57). However, two independent studies using a mouse chimera (58) or a conditional knock-out of Npc1 (51) have demonstrated cell autonomous death of Purkinje neurons. Additionally, neuron-targeted Npc1 gene expression was able to protect neurons and prolonged lifespan in Npc-null mice (59), suggesting that the loss of Npc1 function in neurons rather than glia may be responsible for the loss of neurons in ANPC mice.

At present, the precise mechanism that may underlie degeneration of neurons in either AD or NPC brain remains unclear, but there is evidence of up-regulation of lysosomal enzymes in 'at-risk' neurons in both the diseases (7,60). This is substantiated by our study, which shows an increased level and activity of the cathepsin D both in the hippocampus and cerebellum of ANPC and Npc-null mice. Our subcellular data, on the other hand, show that cytosolic levels of cathepsin D are markedly increased in the cerebellum, but only slightly increased in the relatively spared hippocampus of Npc-null and ANPC mice compared with WT controls. This is accompanied by a parallel increase in the cytosolic levels of cytochrome c and Bax in the cerebellum of Npc-null and ANPC mice. The

magnitude of cytosolic cathepsin D levels, in keeping with the loss of neurons, is found to be markedly higher in ANPC than Npc-null mice. There is evidence that increased activity of enzymes within lysosomes or limited release of enzymes into the cytosol can prevent sub-lethal damage, whereas sustained release of the enzymes into the cytosol can induce cell death (43,45). Thus, it is likely that enhanced levels of cathepsin D in the hippocampus may counter cellular abnormalities resulting from APP overexpression/cholesterol accumulation or may not reach levels necessary to mediate cell death. On the other hand, larger increases in cytosolic levels of the enzyme in the cerebellum, resulting from lysosomal destabilization, may lead to death of neurons. This is supported by two lines of evidence: (i) Purkinje cells, but not hippocampal neurons, are labeled with cleaved caspase-3 in ANPC and Npc-null mice and (ii) cytosolic cathepsin D levels did not differ in hippocampus or cerebellum among APP-Tg, Dhet and WT mice, which do not exhibit any loss of neurons.

Apart from lysosomal dysfunction, the presence of tau-positive NFTs represents a striking similarity between AD and NPC pathologies (15,16). The formation of tangles resulting from phosphorylation of tau protein has been implicated in the degeneration of neurons in many taupathies including NPC and AD brains by triggering loss of microtubule binding and impaired axonal transport (61). Tau phosphorylation is usually mediated in a site-specific manner by various kinases including ERK1/2, GSK-3b and Cdk-5 (62,63). Although tau is known to be phosphorylated in APP-Tg and Npc-null mice, there is no evidence of its association with the loss of neurons or tangle formation in any region of the brain (64–66). Our results clearly show that while the total-tau levels are decreased, phospho-tau levels in relation to total tau are increased in the cerebellum but not in the hippocampus of ANPC and Npc-null mice. These changes are significantly higher in ANPC than Npc-null mice and are accompanied by an increase in phospho-ERK1/2 and a decrease in p35 levels. Since partial or complete loss of tau expression can reduce lifespan and exacerbate pathology in Npc-null mice (67) and inhibitors of Cdk-5 can attenuate tau phosphorylation as well as the phenotype in Npc-null mice (37,68), it is likely that alterations in the levels and phosphorylation of tau in the cerebellum of ANPC and Npc-null mice may be involved in the loss of Purkinje neurons. Additionally, we showed that caspase-cleaved tau levels are selectively increased and expressed in the Purkinje neurons of ANPC and Npc-null mice. Since truncated tau generated by caspases tends to assemble more rapidly into filaments than full-length tau (69,70) and is able to trigger neurodegeneration by reducing the pool of full-length tau available for binding to microtubules (40–42), it is likely that cleaved tau in ANPC and Npc-null mice may also contribute to the loss of Purkinje neurons.

Since neuropathological abnormalities in mutant ANPC mice were evident primarily in brain regions that are preferentially vulnerable to cholesterol accumulation in NPC pathology, we treated the animals with 2-HPC—which binds to cholesterol and facilitates its exit from lysosomes even in the absence of functional Npc1 protein (71). A number of recent studies have shown that single or repeated administration of 2-HPC can increase lifespan, delay motor impairments and reduce neuronal cholesterol accumulation in Npc-null mice. Additionally, 2-HPC treatment is able to attenuate degeneration of neurons as well as glial pathology in Npc-null mice (33–35,72). Our results also clearly show that single systemic administration of 2-HPC at postnatal day 7 can not only prevent cholesterol accumulation but also prolong the lifespan and attenuate both motor and object recognition memory deficits in ANPC and Npc-null mice. Additionally, a marked reduction in the glial pathology and protection of Purkinje cells are apparent in 2-HPC-treated ANPC and Npc-null mice compared with the respective saline-treated mice. These cellular changes are accompanied by a significant reversal of phospho-ERK1/2 levels as well as phosphorylation and cleavage of tau in the cerebellum of ANPC and Npc-null mice. Given the beneficial effects of a single injection, it would be of interest to determine whether repeated injections of 2-HPC over time can completely prevent the dysfunction associated with ANPC mice. Nevertheless, our results clearly show that overexpression of APP in Npc-null mice can negatively influence longevity as well as a spectrum of behavioral and neuropathological features that can be reversed markedly by 2-HPC treatment. Additionally, this study raises the possibility of a functional interaction between APP and NPC1 that may have a role in the development of both AD and NPC diseases.

MATERIALS AND METHODS

Materials

Four to twenty percent Tris–Glycine gels, 4–12% NuPAGE Bis–Tris gels, NeuroTrace red fluorescent Nissl stain (BrainStain^{TM} Imaging Kit), Alexa Fluor 488/594 conjugated secondary antibodies and ProLong Gold antifade reagent were all purchased from Life technologies. The DNA isolation kit and Qproteome cell compartment kit were from Qiagen Inc. Filipin, the cathepsin D assay kit, and 2-HPC (product H107) were obtained from Sigma-Aldrich, Inc. The bicinchoninic acid (BCA) protein assay kit and the enhanced chemiluminescence (ECL) kit were obtained from ThermoFisher Scientific. Sources of all the primary antibodies used in the study are listed in Table 1. All horseradish peroxidase (HRP)-conjugated secondary antibodies were purchased from Santa Cruz Biotechnology, Inc. All other chemicals were from Sigma-Aldrich or ThermoFisher Scientific.

Generation of transgenic mice

Mutant human $APP_{KM670/671NL+V717F}$ transgenic mice (APP-Tg) maintained on a C3H/C57BL6 background (29) were obtained from our breeding colony. Heterozygous Npc1-deficient ($Npc1^{+/-}$) mice (32) maintained on a BALB/c background were purchased from Jackson Laboratories. Mutant APP-Tg mice were first crossed to $Npc1^{+/-}$ mice to produce $APP^{+/0}Npc1^{+/-}$ and $APP^{0/0}Npc1^{+/-}$ off-springs. These two lines of mice were subsequently crossed to generate the following five lines of mice: bigenic $APP^{+/0}Npc1^{-/-}$ (ANPC), $APP^{+/0}Npc1^{+/+}$ (APP-Tg), $APP^{0/0}Npc1^{-/-}$ (Npc-null), $APP^{+/0}Npc1^{+/-}$ (double heterozygous: Dhet) and $APP^{0/0}Npc1^{+/+}$ (wild-type, WT), all on a C3H/C57BL6/BALB/c background. Animals of different genotypes used in a given experiment were obtained from the same breeding pairs. All animals, maintained on a 12 h light/dark cycle,

Table 1. Details of the primary antibodies used in this study

Antibody	Type	IHC/IF dilution	WB dilution	Source
Apoptosis inducing factor (AIF)	Polyclonal	n/a	1:200	Santa Cruz Biotechnology, Inc.
Amyloid precursor protein (APP, clone Y188)	Monoclonal	n/a	1:5000	Abcam®
AT-8	Monoclonal	n/a	1:1000	ThermoFisher Scientific
AT-100	Monoclonal	n/a	1:1000	ThermoFisher Scientific
AT-180	Monoclonal	n/a	1:1000	ThermoFisher Scientific
AT-270	Monoclonal	n/a	1:1000	ThermoFisher Scientific
Bcl-2-associated X protein (Bax)	Monoclonal	n/a	1:200	Santa Cruz Biotechnology, Inc.
Calbindin-D-28K	Monoclonal	1:7000	n/a	Sigma-Aldrich, Inc.
Cathepsin D	Polyclonal	n/a	1:200	Santa Cruz Biotechnology, Inc.
Cleaved caspase-3	Monoclonal	1:200	n/a	Cell Signaling Technology
2′,3′-Cyclic nucleotide 3′-phosphodiesterase (CNPase)	Monoclonal	1:500	1:1000	EMD Millipore, Co.
Cyclin dependent kinase 5 (Cdk5)	Monoclonal	n/a	1:200	Santa Cruz Biotechnology, Inc.
Cytochrome c	Monoclonal	n/a	1:1000	BD Transduction Laboratories™
Glial fibrillary acidic protein (GFAP)	Polyclonal	1:1000	1:1000	Dako
Glyceraldehyde-3-phosphate dehydrogenase (GAPDH)	Monoclonal	n/a	1:1000	Sigma-Aldrich, Inc.
Glycogen synthase kinase-3β (GSK-3β)	Monoclonal	n/a	1:5000	BD Transduction Laboratories™
Histone H3	Polyclonal	n/a	1:500	Santa Cruz Biotechnology, Inc.
Ionizing calcium-binding adaptor molecule 1 (Iba1)	Polyclonal	1:3000	1:1000	Wako Chemicals, Inc.
N-cadherin	Polyclonal	n/a	1:200	Santa Cruz Biotechnology, Inc.
Niemann-Pick Type C1 (NPC1)	Polyclonal	n/a	1:1000	Abcam®
p35	Polyclonal	n/a	1:200	Santa Cruz Biotechnology, Inc.
Extracellular signal-regulated kinase 1/2 (ERK1/2)	Monoclonal	n/a	1:2000	Cell Signaling Technology, Inc.
PHF1 Tau	Monoclonal	n/a	1:1000	Kind gift from Dr. Peter Davis
Phospho-Thr^{202}/Tyr^{204} ERK1/2 (Phospho-ERK1/2)	Polyclonal	n/a	1:1000	Cell Signaling Technology, Inc.
Phospho-Tyr^{216}GSK-3	Monoclonal	n/a	1:1000	Upstate Biotechnology Inc.
Postsynaptic density protein 95 (PSD95)	Monoclonal	n/a	1:500	EMD Millipore, Co.
Synaptophysin	Monoclonal	n/a	1:3000	Sigma-Aldrich, Inc.
Tau, caspase cleaved	Monoclonal	1:100	1:1000	EMD Millipore, Co.
Tau-1	Monoclonal	n/a	1:1000	EMD Millipore, Co.
Tau-5	Monoclonal	n/a	1:2000	EMD Millipore, Co.
β-Actin	Monoclonal	n/a	1:5000	Sigma-Aldrich, Inc.

IHC/IF, immunohistochemistry/immunofluorescence; WB, western blotting; n/a, not used in that specific application.

were bred and housed with access to food and water *ad libitum*. The probability of survival was determined by the Kaplan–Meier technique using GraphPad Prism software. The maintenance of the breeding colony and the experiments involving these animals were performed in accordance with Institutional and Canadian Council on Animal Care guidelines. All transgenic mice were identified by a unique ear notching pattern and genotyped by PCR analysis of tail DNA as described earlier (29,32).

Behavioral tests

WT, APP-Tg, Dhet, Npc-null and ANPC mice were examined at 4, 7 and 10 weeks of age for their object recognition memory and sensorimotor performance as described earlier (73). All these mice were generated from the same breeding on a C3H/C57BL6/BALB/c background, thus making it likely that behavioral changes observed in any of these lines may be associated with altered expression of APP and/or Npc1 rather than with the background strains. For the object recognition memory test, mice were first habituated for five consecutive days and on the sixth day their exploratory behavior towards a familiar and novel object was quantified using a MI, wherein 't_o' represents the time exploring an object during the original exposure and 't_n' represents the time spent exploring an object that is novel on re-exposure: $\mathrm{MI} = (t_n - t_o)/(t_n + t_o)$. The motor function of mice from different genotypes was tested by measurement of latency to fall from a Rotamex-5 accelerating rotarod (Columbus Instruments). All mice were examined 5 min each four times per day with an inter-trial interval of 30 min for five consecutive days. A score of 300 s was assigned to a mouse that stayed on the rod for the full 5 min test period. Gait analysis of the animals was done from their footprints as described earlier (74). Stride lengths and hind limb widths were measured manually as the distance between two paw prints. Mice of different genotypes were also tested for their open-field activity over a 5-min test session. Durations of walking, pausing and rearing were analyzed as indices of spontaneous locomotor activity as described earlier (73).

Cellular cholesterol assay

The hippocampus and cerebellum of 4-, 7- and 10-week mice of all five genotypes ($n = 4$ per genotype/age group) were homogenized and mass of cholesterol was determined using gas–liquid chromatography as described earlier (44).

Histology and Immunohistochemistry

WT, APP-Tg, Dhet, Npc-null and ANPC mice of 4, 7 and 10 weeks ($n = 4$–5 per genotype/age group) were transcardially

perfused and fixed in 4% paraformaldehyde. Brains were sectioned on a cryostat (20 μm) and then processed as described earlier (5). To determine cholesterol accumulation, brain sections from all five genotypes were incubated with 25 μg/ml of filipin in phosphate buffered saline for 30 min in the dark under agitation (5). For immunohistochemistry, sections were incubated overnight at 4°C with the anti-GFAP, anti-Iba1, anti-CNPase, anti-Calbindin-D-28k, anti-cleaved caspase-3 or anti-Tau, caspase cleaved antibodies at dilutions listed in Table 1. Subsequently, sections were incubated with appropriate HRP-conjugated secondary antibodies (1:400) for enzyme-linked immunohistochemistry or Alexa Fluor 488/594-conjugated secondary antibodies (1:1000) for immunofluorescence methods. Immunostained sections were examined and photographed using a Zeiss Axioskop-2 microscope (Carl Zeiss Canada Ltd.).

Neuronal cell counting

For neuronal quantification, every sixth section from the hippocampus and cerebellum of 7-week-old mice of different genotypes were used ($n = 3$ to 4 per genotype). Hippocampal sections were stained with NeuroTrace 530/616 red fluorescent Nissl stain (1:300), whereas cerebellar Purkinje cells were labeled using anti-calbindin D-28k antiserum as mentioned above. Cell counts were normalized to the CA1 area or the Purkinje layer length and expressed as neuronal density as described earlier (51).

Western blotting

Hippocampal and cerebellar brain regions were homogenized in ice-cold RIPA lysis buffer and protein content was determined using a BCA protein assay kit as described earlier (5). Equal amounts of protein samples were separated on 4–20% Tris-Glycine gels or 4–12% NuPAGE Bis-Tris gels and transferred to nitrocellulose membranes, blocked with 5% non-fat milk and then incubated overnight at 4°C with either anti-APP, anti-NPC1, anti-GFAP, anti-Iba1, anti-CNPase, anti-PSD95, anti-synaptophysin, anti-cathepsin D, anti-AT100, anti-PHF1, anti-AT8, anti-AT180, anti-AT270, anti-Tau-5, anti-Tau-1, anti-Tau, caspase cleaved, anti-phospho-Thr^{202}/Tyr^{204} ERK1/2, anti-ERK1/2, anti-Cdk5, anti-p35, anti-phospho-Tyr^{216}GSK3 or anti-total GSK-3β antisera at dilutions listed in Table 1. On the following day, membranes were washed, incubated with appropriate HRP-conjugated secondary antibodies (1:5000) and immunoreactive proteins were visualized using an ECL detection kit. All Blots were re-probed with anti-β-actin antibody and quantified using a MCID image analyzer.

Cathepsin D activity assay

Hippocampus and cerebellum of 7-week-old WT, APP-Tg, Dhet, Npc-null and ANPC mice ($n = 4–8$ per genotype) were homogenized and centrifuged at 4°C for 10 min. The supernatant was assayed to determine the protein content and then used to measure the cathepsin D activity using the fluorogenic assay kit according to the manufacturer's instructions.

Subcellular fractionation

Hippocampus and cerebellum of 7-week-old WT, APP-Tg, Dhet, Npc-null and ANPC mice ($n = 3–4$ per genotype) were homogenized in ice-cold PBS and fractionated using the Qproteome cell compartment kit into cytosol, membrane and nuclear fractions. The protein content of different fractions was determined using a BCA protein assay kit and equal amounts of protein were separated by sodium dodecyl sulphate-polyacrylamide gel electrophoresis (SDS-PAGE). Immunoblotting was performed with anti-cathepsin D, anti-cytochrome c, anti-Bax and anti-AIF antisera as mentioned earlier (44). All blots were re-probed with anti-glyceraldehyde-3-phosphate dehydrogenase (anti-GAPDH), anti-N-cadherin and anti-histone antibodies to check for equal protein loading for the cytosolic, membrane and nuclear fractions, respectively.

2-HPC treatment

A subset of WT, Npc-null and ANPC mice were administered a single subcutaneous injection of either 2-HPC (4000 mg/kg body weight; 20% wt/vol in saline solution; $n = 14–16$ per genotype) or normal saline ($n = 9–12$ per genotype) at 7 days of age at the scruff of the neck as described recently (34). Following treatment, a subset of mice from saline- and 2HPC-treated groups were kept to determine their longevity, whereas another subgroup were tested for object recognition memory and rotarod performance using protocols described above. In parallel, brains from saline- and drug-treated mice were collected and processed for histology, immunohistochemistry or immunoblotting as described above.

Statistical analysis

All data are presented as means ± SEM. Statistical differences between the different genotype combinations were tested using one-way ANOVA followed by Newman–Keuls multiple comparison *post-hoc* analysis (Graph-Pad Software, Inc.) with significance set at $P < 0.05$. Differences among survival curves were determined using the log-rank test, whereas statistical differences between saline-and 2-HPC-treated Npc-null or ANPC mice were tested using the unpaired Student's *t*-test with significance set at $P < 0.05$.

SUPPLEMENTARY MATERIAL

Supplementary Material is available at *HMG* online.

ACKNOWLEDGEMENTS

This work was supported by grants from Canadian Institutes of Health Research (MOP-97837) and University Hospital Foundation (RES0012321). M.M. is a recipient of a President's Doctoral Award from the University of Alberta and a Studentship Award from the Alberta Heritage Foundation for Medical Research (AHFMR). Y.W. is a recipient of Studentship Award from AHFMR. S.K. is a recipient of a Canada Research Chair (Tier-II) in Neurodegenerative Diseases. D.W. is a recipient of a Canada Research Chair (Tier-I) in Medicine and a Scientist Award from AHFMR.

Conflict of Interest statement. None declared.

REFERENCES

1. Mukherjee, S. and Maxfield, F.R. (2004) Lipid and cholesterol trafficking in NPC. *Biochim. Biophys. Acta*, **1685**, 28–37.
2. Pacheco, C.D. and Lieberman, A.P. (2008) The pathogenesis of Niemann-Pick type C disease: a role for autophagy? *Expert Rev. Mol. Med.*, **10**, e26.
3. Carstea, E.D., Morris, J.A., Coleman, K.G., Loftus, S.K., Zhang, D., Cummings, C., Gu, J., Rosenfeld, M.A., Pavan, W.J., Krizman, D.B. *et al.* (1997) Niemann-Pick C1 disease gene: homology to mediators of cholesterol homeostasis. *Science*, **277**, 228–231.
4. Walkley, S.U. and Suzuki, K. (2004) Consequences of NPC1 and NPC2 loss of function in mammalian neurons. *Biochim. Biophys. Acta*, **1685**, 48–62.
5. Kodam, A., Maulik, M., Peake, K., Amritraj, A., Vetrivel, K.S., Thinakaran, G., Vance, J.E. and Kar, S. (2010) Altered levels and distribution of amyloid precursor protein and its processing enzymes in Niemann-Pick type C1-deficient mouse brains. *Glia*, **58**, 1267–1281.
6. Li, H., Repa, J.J., Valasek, M.A., Beltroy, E.P., Turley, S.D., German, D.C. and Dietschy, J.M. (2005) Molecular, anatomical, and biochemical events associated with neurodegeneration in mice with Niemann-Pick type C disease. *J. Neuropathol. Exp. Neurol.*, **64**, 323–333.
7. Jin, L.W., Shie, F.S., Maezawa, I., Vincent, I. and Bird, T. (2004) Intracellular accumulation of amyloidogenic fragments of amyloid-beta precursor protein in neurons with Niemann-Pick type C defects is associated with endosomal abnormalities. *Am. J. Pathol.*, **164**, 975–985.
8. Mattsson, N., Zetterberg, H., Bianconi, S., Yanjanin, N.M., Fu, R., Mansson, J.E., Porter, F.D. and Blennow, K. (2011) Gamma-secretase-dependent amyloid-beta is increased in Niemann-Pick type C: a cross-sectional study. *Neurology*, **76**, 366–372.
9. Saito, Y., Suzuki, K., Nanba, E., Yamamoto, T., Ohno, K. and Murayama, S. (2002) Niemann-Pick type C disease: accelerated neurofibrillary tangle formation and amyloid beta deposition associated with apolipoprotein E epsilon 4 homozygosity. *Ann. Neurol.*, **52**, 351–355.
10. Baudry, M., Yao, Y., Simmons, D., Liu, J. and Bi, X. (2003) Postnatal development of inflammation in a murine model of Niemann-Pick type C disease: immunohistochemical observations of microglia and astroglia. *Exp. Neurol.*, **184**, 887–903.
11. German, D.C., Quintero, E.M., Liang, C.L., Ng, B., Punia, S., Xie, C. and Dietschy, J.M. (2001) Selective neurodegeneration, without neurofibrillary tangles, in a mouse model of Niemann-Pick C disease. *J. Comp. Neurol.*, **433**, 415–425.
12. Goate, A. and Hardy, J. (2012) Twenty years of Alzheimer's disease-causing mutations. *J. Neurochem.*, **120**(Suppl. 1), 3–8.
13. Selkoe, D.J. (2008) Biochemistry and molecular biology of amyloid beta-protein and the mechanism of Alzheimer's disease. *Handb. Clin. Neurol.*, **89**, 245–260.
14. St George-Hyslop, P.H., McLaurin, J. and Fraser, P.E. (2000) Neuropathological, biochemical and genetic alterations in AD. *Drug News Perspect.*, **13**, 281–288.
15. Auer, I.A., Schmidt, M.L., Lee, V.M., Curry, B., Suzuki, K., Shin, R.W., Pentchev, P.G., Carstea, E.D. and Trojanowski, J.Q. (1995) Paired helical filament tau (PHFtau) in Niemann-Pick type C disease is similar to PHFtau in Alzheimer's disease. Acta Neuropathol. *(*Berl*)*, **90**, 547–551.
16. Ohm, T.G., Treiber-Held, S., Distl, R., Glockner, F., Schonheit, B., Tamanai, M. and Meske, V. (2003) Cholesterol and tau protein–findings in Alzheimer's and Niemann Pick C's disease. *Pharmacopsychiatry*, **36**(Suppl. 2), S120–126.
17. Kim, J., Basak, J.M. and Holtzman, D.M. (2009) The role of apolipoprotein E in Alzheimer's disease. *Neuron*, **63**, 287–303.
18. Poirier, J., Davignon, J., Bouthillier, D., Kogan, S., Bertrand, P. and Gauthier, S. (1993) Apolipoprotein E polymorphism and Alzheimer's disease. *Lancet*, **342**, 697–699.
19. Nixon, R.A. (2004) Niemann-Pick Type C disease and Alzheimer's disease: the APP-endosome connection fattens up. *Am. J. Pathol.*, **164**, 757–761.
20. Kagedal, K., Kim, W.S., Appelqvist, H., Chan, S., Cheng, D., Agholme, L., Barnham, K., McCann, H., Halliday, G. and Garner, B. (2010) Increased expression of the lysosomal cholesterol transporter NPC1 in Alzheimer's disease. *Biochim. Biophys. Acta*, **1801**, 831–838.
21. Kivipelto, M., Helkala, E.L., Laakso, M.P., Hanninen, T., Hallikainen, M., Alhainen, K., Iivonen, S., Mannermaa, A., Tuomilehto, J., Nissinen, A. *et al.* (2002) Apolipoprotein E epsilon4 allele, elevated midlife total cholesterol level, and high midlife systolic blood pressure are independent risk factors for late-life Alzheimer disease. *Ann. Intern. Med.*, **137**, 149–155.
22. Notkola, I.L., Sulkava, R., Pekkanen, J., Erkinjuntti, T., Ehnholm, C., Kivinen, P., Tuomilehto, J. and Nissinen, A. (1998) Serum total cholesterol, apolipoprotein E epsilon 4 allele, and Alzheimer's disease. *Neuroepidemiology*, **17**, 14–20.
23. Distl, R., Meske, V. and Ohm, T.G. (2001) Tangle-bearing neurons contain more free cholesterol than adjacent tangle-free neurons. Acta Neuropathol. *(*Berl*)*, **101**, 547–554.
24. Fassbender, K., Simons, M., Bergmann, C., Stroick, M., Lutjohann, D., Keller, P., Runz, H., Kuhl, S., Bertsch, T., von Bergmann, K. *et al.* (2001) Simvastatin strongly reduces levels of Alzheimer's disease beta-amyloid peptides Abeta 42 and Abeta 40 in vitro and in vivo. *Proc. Natl Acad. Sci. USA*, **98**, 5856–5861.
25. Grimm, M.O., Grimm, H.S., Tomic, I., Beyreuther, K., Hartmann, T. and Bergmann, C. (2008) Independent inhibition of Alzheimer disease beta- and gamma-secretase cleavage by lowered cholesterol levels. *J. Biol. Chem.*, **283**, 11302–11311.
26. Martin, M., Dotti, C.G. and Ledesma, M.D. (2010) Brain cholesterol in normal and pathological aging. *Biochim. Biophys. Acta*, **1801**, 934–944.
27. Refolo, L.M., Pappolla, M.A., LaFrancois, J., Malester, B., Schmidt, S.D., Thomas-Bryant, T., Tint, G.S., Wang, R., Mercken, M., Petanceska, S.S. *et al.* (2001) A cholesterol-lowering drug reduces beta-amyloid pathology in a transgenic mouse model of Alzheimer's disease. *Neurobiol. Dis.*, **8**, 890–899.
28. Adalbert, R., Nogradi, A., Babetto, E., Janeckova, L., Walker, S.A., Kerschensteiner, M., Misgeld, T. and Coleman, M.P. (2009) Severely dystrophic axons at amyloid plaques remain continuous and connected to viable cell bodies. *Brain*, **132**, 402–416.
29. Chishti, M.A., Yang, D.S., Janus, C., Phinney, A.L., Horne, P., Pearson, J., Strome, R., Zuker, N., Loukides, J., French, J. *et al.* (2001) Early-onset amyloid deposition and cognitive deficits in transgenic mice expressing a double mutant form of amyloid precursor protein 695. *J. Biol. Chem.*, **276**, 21562–21570.
30. Francis, B.M., Kim, J., Barakat, M.E., Fraenkl, S., Yucel, Y.H., Peng, S., Michalski, B., Fahnestock, M., McLaurin, J. and Mount, H.T. (2012) Object recognition memory and BDNF expression are reduced in young TgCRND8 mice. *Neurobiol. Aging*, **33**, 555–563.
31. Reddy, P.H. (2011) Abnormal tau, mitochondrial dysfunction, impaired axonal transport of mitochondria, and synaptic deprivation in Alzheimer's disease. *Brain Res.*, **1415**, 136–148.
32. Loftus, S.K., Morris, J.A., Carstea, E.D., Gu, J.Z., Cummings, C., Brown, A., Ellison, J., Ohno, K., Rosenfeld, M.A., Tagle, D.A. *et al.* (1997) Murine model of Niemann-Pick C disease: mutation in a cholesterol homeostasis gene. *Science*, **277**, 232–235.
33. Davidson, C.D., Ali, N.F., Micsenyi, M.C., Stephney, G., Renault, S., Dobrenis, K., Ory, D.S., Vanier, M.T. and Walkley, S.U. (2009) Chronic cyclodextrin treatment of murine Niemann-Pick C disease ameliorates neuronal cholesterol and glycosphingolipid storage and disease progression. *PLoS One*, **4**, e6951.
34. Liu, B., Turley, S.D., Burns, D.K., Miller, A.M., Repa, J.J. and Dietschy, J.M. (2009) Reversal of defective lysosomal transport in NPC disease ameliorates liver dysfunction and neurodegeneration in the npc1−/− mouse. *Proc. Natl Acad. Sci. USA*, **106**, 2377–2382.
35. Ramirez, C.M., Liu, B., Taylor, A.M., Repa, J.J., Burns, D.K., Weinberg, A.G., Turley, S.D. and Dietschy, J.M. (2010) Weekly cyclodextrin administration normalizes cholesterol metabolism in nearly every organ of the Niemann-Pick type C1 mouse and markedly prolongs life. *Pediatr. Res.*, **68**, 309–315.
36. Liu, B., Li, H., Repa, J.J., Turley, S.D. and Dietschy, J.M. (2008) Genetic variations and treatments that affect the lifespan of the NPC1 mouse. *J. Lipid Res.*, **49**, 663–669.
37. Hao, Y., Pan, D., Zhang, M., Xu, J., Li, L., Wei, J. and Wang, X. (2009) The neuroprotective effects of cyclin-dependent kinase-5 inhibition in mice with Niemann-Pick disease type C. *J. Huazhong Univ. Sci. Technolog. Med. Sci.*, **29**, 324–329.
38. Ahmad, I., Lope-Piedrafita, S., Bi, X., Hicks, C., Yao, Y., Yu, C., Chaitkin, E., Howison, C.M., Weberg, L., Trouard, T.P. *et al.* (2005) Allopregnanolone treatment, both as a single injection or repetitively,

delays demyelination and enhances survival of Niemann-Pick C mice. *J. Neurosci. Res.*, **82**, 811–821.
39. Ohm, T.G. and Meske, V. (2006) Cholesterol, statins and tau. *Acta Neurol. Scand. Suppl.*, **185**, 93–101.
40. Guillozet-Bongaarts, A.L., Glajch, K.E., Libson, E.G., Cahill, M.E., Bigio, E., Berry, R.W. and Binder, L.I. (2007) Phosphorylation and cleavage of tau in non-AD tauopathies. Acta Neuropathol. *(*Berl*)*, **113**, 513–520.
41. Park, S.Y. and Ferreira, A. (2005) The generation of a 17kDa neurotoxic fragment: an alternative mechanism by which tau mediates beta-amyloid-induced neurodegeneration. *J. Neurosci.*, **25**, 5365–5375.
42. Wang, Y., Garg, S., Mandelkow, E.M. and Mandelkow, E. (2010) Proteolytic processing of tau. *Biochem. Soc. Trans.*, **38**, 955–961.
43. Bendiske, J. and Bahr, B.A. (2003) Lysosomal activation is a compensatory response against protein accumulation and associated synaptopathogenesis–an approach for slowing Alzheimer disease? *J. Neuropathol. Exp. Neurol.*, **62**, 451–463.
44. Amritraj, A., Peake, K., Kodam, A., Salio, C., Merighi, A., Vance, J.E. and Kar, S. (2009) Increased activity and altered subcellular distribution of lysosomal enzymes determine neuronal vulnerability in Niemann-Pick type C1-deficient mice. *Am. J. Pathol.*, **175**, 2540–2556.
45. Chwieralski, C.E., Welte, T. and Buhling, F. (2006) Cathepsin-regulated apoptosis. *Apoptosis*, **11**, 143–149.
46. Turk, B., Stoka, V., Rozman-Pungercar, J., Cirman, T., Droga-Mazovec, G., Oresic, K. and Turk, V. (2002) Apoptotic pathways: involvement of lysosomal proteases. *Biol. Chem.*, **383**, 1035–1044.
47. Martins, I.J., Berger, T., Sharman, M.J., Verdile, G., Fuller, S.J. and Martins, R.N. (2009) Cholesterol metabolism and transport in the pathogenesis of Alzheimer's disease. *J. Neurochem.*, **111**, 1275–1308.
48. Kuzyk, A., Kastyak, M., Agrawal, V., Gallant, M., Sivakumar, G., Rak, M., Del Bigio, M.R., Westaway, D., Julian, R. and Gough, K.M. (2010) Association among amyloid plaque, lipid, and creatine in hippocampus of TgCRND8 mouse model for Alzheimer disease. *J. Biol. Chem.*, **285**, 31202–31207.
49. Halford, R.W. and Russell, D.W. (2009) Reduction of cholesterol synthesis in the mouse brain does not affect amyloid formation in Alzheimer's disease, but does extend lifespan. *Proc. Natl Acad. Sci. USA*, **106**, 3502–3506.
50. Burwell, R.D., Saddoris, M.P., Bucci, D.J. and Wiig, K.A. (2004) Corticohippocampal contributions to spatial and contextual learning. *J. Neurosci.*, **24**, 3826–3836.
51. Elrick, M.J., Pacheco, C.D., Yu, T., Dadgar, N., Shakkottai, V.G., Ware, C., Paulson, H.L. and Lieberman, A.P. (2010) Conditional Niemann-Pick C mice demonstrate cell autonomous Purkinje cell neurodegeneration. *Hum. Mol. Genet.*, **19**, 837–847.
52. Middleton, F.A. and Strick, P.L. (1998) Cerebellar output: motor and cognitive channels. *Trends Cogn. Sci.*, **2**, 348–354.
53. German, D.C., Liang, C.L., Song, T., Yazdani, U., Xie, C. and Dietschy, J.M. (2002) Neurodegeneration in the Niemann-Pick C mouse: glial involvement. *Neuroscience*, **109**, 437–450.
54. Stein, T.D. and Johnson, J.A. (2002) Lack of neurodegeneration in transgenic mice overexpressing mutant amyloid precursor protein is associated with increased levels of transthyretin and the activation of cell survival pathways. *J. Neurosci.*, **22**, 7380–7388.
55. Chen, G., Li, H.M., Chen, Y.R., Gu, X.S. and Duan, S. (2007) Decreased estradiol release from astrocytes contributes to the neurodegeneration in a mouse model of Niemann-Pick disease type C. *Glia*, **55**, 1509–1518.
56. Lloyd-Evans, E., Morgan, A.J., He, X., Smith, D.A., Elliot-Smith, E., Sillence, D.J., Churchill, G.C., Schuchman, E.H., Galione, A. and Platt, F.M. (2008) Niemann-Pick disease type C1 is a sphingosine storage disease that causes deregulation of lysosomal calcium. *Nat. Med.*, **14**, 1247–1255.
57. Zhang, M., Strnatka, D., Donohue, C., Hallows, J.L., Vincent, I. and Erickson, R.P. (2008) Astrocyte-only Npc1 reduces neuronal cholesterol and triples life span of Npc1−/− mice. *J. Neurosci. Res.*, **86**, 2848–2856.
58. Ko, D.C., Milenkovic, L., Beier, S.M., Manuel, H., Buchanan, J. and Scott, M.P. (2005) Cell-autonomous death of cerebellar purkinje neurons with autophagy in Niemann-Pick type C disease. *PLoS Genet.*, **1**, 81–95.
59. Lopez, M.E., Klein, A.D., Dimbil, U.J. and Scott, M.P. (2011) Anatomically defined neuron-based rescue of neurodegenerative Niemann-Pick type C disorder. *J. Neurosci.*, **31**, 4367–4378.
60. Nixon, R.A. and Cataldo, A.M. (2006) Lysosomal system pathways: genes to neurodegeneration in Alzheimer's disease. *J. Alzheimers Dis.*, **9**, 277–289.
61. Morris, M., Maeda, S., Vossel, K. and Mucke, L. (2011) The many faces of tau. *Neuron*, **70**, 410–426.
62. Ballatore, C., Lee, V.M. and Trojanowski, J.Q. (2007) Tau-mediated neurodegeneration in Alzheimer's disease and related disorders. *Nat. Rev. Neurosci.*, **8**, 663–672.
63. Dolan, P.J. and Johnson, G.V. (2010) The role of tau kinases in Alzheimer's disease. *Curr. Opin. Drug Discov. Devel.*, **13**, 595–603.
64. Bellucci, A., Rosi, M.C., Grossi, C., Fiorentini, A., Luccarini, I. and Casamenti, F. (2007) Abnormal processing of tau in the brain of aged TgCRND8 mice. *Neurobiol. Dis.*, **27**, 328–338.
65. Bu, B., Li, J., Davies, P. and Vincent, I. (2002) Deregulation of Cdk5, hyperphosphorylation, and cytoskeletal pathology in the Niemann-Pick type C murine model. *J. Neurosci.*, **22**, 6515–6525.
66. Sawamura, N., Gong, J.S., Garver, W.S., Heidenreich, R.A., Ninomiya, H., Ohno, K., Yanagisawa, K. and Michikawa, M. (2001) Site-specific phosphorylation of tau accompanied by activation of mitogen-activated protein kinase (MAPK) in brains of Niemann-Pick type C mice. *J. Biol. Chem.*, **276**, 10314–10319.
67. Pacheco, C.D., Elrick, M.J. and Lieberman, A.P. (2009) Tau deletion exacerbates the phenotype of Niemann-Pick type C mice and implicates autophagy in pathogenesis. *Hum. Mol. Genet.*, **18**, 956–965.
68. Zhang, M., Li, J., Chakrabarty, P., Bu, B. and Vincent, I. (2004) Cyclin-dependent kinase inhibitors attenuate protein hyperphosphorylation, cytoskeletal lesion formation, and motor defects in Niemann-Pick Type C mice. *Am. J. Pathol.*, **165**, 843–853.
69. Liu, M.C., Kobeissy, F., Zheng, W., Zhang, Z., Hayes, R.L. and Wang, K.K. (2011) Dual vulnerability of tau to calpains and caspase-3 proteolysis under neurotoxic and neurodegenerative conditions. *A.S.N. Neuro.*, **3**, e00051.
70. Rissman, R.A., Poon, W.W., Blurton-Jones, M., Oddo, S., Torp, R., Vitek, M.P., LaFerla, F.M., Rohn, T.T. and Cotman, C.W. (2004) Caspase-cleavage of tau is an early event in Alzheimer disease tangle pathology. *J. Clin. Invest.*, **114**, 121–130.
71. Rosenbaum, A.I. and Maxfield, F.R. (2011) Niemann-Pick type C disease: molecular mechanisms and potential therapeutic approaches. *J. Neurochem.*, **116**, 789–795.
72. Aqul, A., Liu, B., Ramirez, C.M., Pieper, A.A., Estill, S.J., Burns, D.K., Repa, J.J., Turley, S.D. and Dietschy, J.M. (2011) Unesterified cholesterol accumulation in late endosomes/lysosomes causes neurodegeneration and is prevented by driving cholesterol export from this compartment. *J. Neurosci.*, **31**, 9404–9413.
73. Vaucher, E., Fluit, P., Chishti, M.A., Westaway, D., Mount, H.T. and Kar, S. (2002) Object recognition memory and cholinergic parameters in mice expressing human presenilin 1 transgenes. *Exp. Neurol.*, **175**, 398–406.
74. D'Hooge, R., Hartmann, D., Manil, J., Colin, F., Gieselmann, V. and De Deyn, P.P. (1999) Neuromotor alterations and cerebellar deficits in aged arylsulfatase A-deficient transgenic mice. *Neurosci. Lett.*, **273**, 93–96.